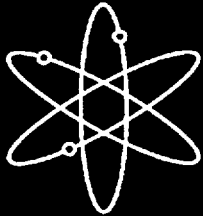
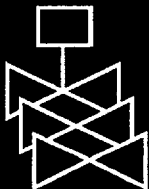


Fracture Toughness Testing With Cracked Round Bars: Feasibility Study



SRI International

Oak Ridge National Laboratory



**U.S. Nuclear Regulatory Commission
Office of Nuclear Regulatory Research
Washington, DC 20555-0001**



AVAILABILITY NOTICE

Availability of Reference Materials Cited in NRC Publications

NRC publications in the NUREG series, NRC regulations, and *Title 10, Energy*, of the *Code of Federal Regulations*, may be purchased from one of the following sources:

1. The Superintendent of Documents
U.S. Government Printing Office
P.O. Box 37082
Washington, DC 20402-9328
<http://www.access.gpo.gov/su_docs>
202-512-1800
2. The National Technical Information Service
Springfield, VA 22161-0002
<<http://www.ntis.gov>>
1-800-553-6847 or locally 703-605-6000

The NUREG series comprises (1) brochures (NUREG/BR-XXXX), (2) proceedings of conferences (NUREG/CP-XXXX), (3) reports resulting from international agreements (NUREG/IA-XXXX), (4) technical and administrative reports and books [(NUREG-XXXX) or (NUREG/CR-XXXX)], and (5) compilations of legal decisions and orders of the Commission and Atomic and Safety Licensing Boards and of Office Directors' decisions under Section 2.206 of NRC's regulations (NUREG-XXXX).

A single copy of each NRC draft report for comment is available free, to the extent of supply, upon written request as follows:

Address: Office of the Chief Information Officer
Reproduction and Distribution
Services Section
U.S. Nuclear Regulatory Commission
Washington, DC 20555-0001
E-mail: <DISTRIBUTION@nrc.gov>
Facsimile: 301-415-2289

A portion of NRC regulatory and technical information is available at NRC's World Wide Web site:

<<http://www.nrc.gov>>

After January 1, 2000, the public may electronically access NUREG-series publications and other NRC records in NRC's Agencywide Document Access and Management System (ADAMS), through the Public Electronic Reading Room (PERR), link <<http://www.nrc.gov/NRC/ADAMS/index.html>>.

Publicly released documents include, to name a few, NUREG-series reports; *Federal Register* notices; applicant, licensee, and vendor documents and correspondence; NRC correspondence and internal memoranda; bulletins and information notices; inspection and investigation reports; licensee event reports; and Commission papers and their attachments.

Documents available from public and special technical libraries include all open literature items, such as books, journal articles, and transactions, *Federal Register* notices, Federal and State legislation, and congressional reports. Such documents as theses, dissertations, foreign reports and translations, and non-NRC conference proceedings may be purchased from their sponsoring organization.

Copies of industry codes and standards used in a substantive manner in the NRC regulatory process are maintained at the NRC Library, Two White Flint North, 11545 Rockville Pike, Rockville, MD 20852-2738. These standards are available in the library for reference use by the public. Codes and standards are usually copyrighted and may be purchased from the originating organization or, if they are American National Standards, from—

American National Standards Institute
11 West 42nd Street
New York, NY 10036-8002
<<http://www.ansi.org>>
212-642-4900

DISCLAIMER

This report was prepared as an account of work sponsored by an agency of the United States Government. Neither the United States Government nor any agency thereof, nor any of their employees, makes any warranty, expressed or implied, or assumes

any legal liability or responsibility for any third party's use, or the results of such use, of any information, apparatus, product, or process disclosed in this report, or represents that its use by such third party would not infringe privately owned rights.

Fracture Toughness Testing with Cracked Round Bars: Feasibility Study

Manuscript Completed: March 2000
Date Published: April 2000

Prepared by
J.H. Giovanola, J.E. Crocker

SRI International
Poulter Laboratory
333 Ravenswood Avenue
Menlo Park, CA 94025

Under Contract to:
Oak Ridge National Laboratory
Managed by Lockheed Martin Energy Research Corporation
Oak Ridge, TN 37831-6158

C.J. Fairbanks, NRC Project Manager

Prepared for
Division of Engineering Technology
Office of Nuclear Regulatory Research
U.S. Nuclear Regulatory Commission
Washington, DC 20555-0001
NRC Job Code L1098



**NUREG/CR-6342 has been
reproduced from the best available copy.**

Abstract

SRI International has investigated the feasibility of measuring representative toughness values for nuclear pressure vessel materials using small cracked round bars (CRBs). We tested a weldment material [Heavy-Section Steel Irradiation (HSSI) Weld 72W with 0.23% copper] at six temperatures (-150° , -80° , -50° , 0° , 23° , and 50°C) using CRBs and compared the fracture-toughness results with data obtained for HSSI Weld 72W by Oak Ridge National Laboratory using 1T-compact tension (CT) specimens.

The overall agreement between the toughness values measured with the CRBs and the 1T-CT was quite good over the entire range of temperatures and for both cleavage and ductile fracture. This agreement attests to the promise of the CRB geometry for providing valid toughness values from small specimens. Nevertheless, we observed some differences, mainly for cleavage toughness values below 0°C . We attribute the differences to (1) possible inaccuracies in the estimation formulas for the J-integral, (2) differences in constraint, and (3) statistical size effects.

We recommend that work be continued to validate the CRB test procedure and to adapt it to specimens that can be fabricated from halves of broken Charpy specimens.

Contents

Abstract	iii
List of Figures	vi
List of Tables	vii
Acknowledgments	ix
Preface	xi
1. Introduction	1
2. Experimental Procedure	3
2.1 Material	3
2.2 Specimen Geometry and Precracking Procedure	3
2.3 Fracture Test Procedure	6
2.4 Fractographic Observations	8
2.5 Data Reduction	8
2.5.1 Displacement Measurements	8
2.5.2 Fracture Initiation Point	9
2.5.3 Estimation of Fracture Toughness	9
3. Experimental Results	11
3.1 Tests at -150°C	11
3.2 Tests at -80°C	11
3.3 Tests at -50°C	13
3.4 Tests at 0°C	18
3.5 Test at 23°C	19
3.6 Tests at 50°C	25
3.7 J-CMOD and J-CTOD Relationships	28
4. Discussion	31
4.1 Comparison of ORNL 1T-CT Data and SRI CRB Data	31
4.2 Significance of $J\text{-}\delta_{\text{cr}}$ Proportionality	34
4.3 Improvement in Experimental Method	34
5. Conclusions and Recommendations	37
5.1 Conclusions	37
5.2 Recommendations	37
6. References	39

Contents (continued)

Appendix A. Composition and Tensile Properties of HSSI Weld 72W (0.23% Copper) Unirradiated	A-1
Appendix B. Analysis of the Effect of Bending on J Values in Cracked Round Bar Experiments	B-1
Appendix C. Analysis of Conditions at Maximum Load in CRB Tests	C-1
Conversion Factors	CF-1

List of Figures

1	Geometry and dimensions of notched round bar specimen	4
2	Rotating fatigue precracking facility	5
3	Stiffness versus uncracked ligament radius for the cracked round bar specimen of Figure 1 under tensile loading	6
4	Experimental arrangement for fracture experiments at temperatures below room temperature	7
5	Load versus displacement curves for experiments with loading	9
6	Load versus crack displacement for fracture experiments at -150°C	12
7	SEM photographs of Specimen B-04 tested at -80°C	14
8	Load versus crack displacement for fracture experiments at -80°C	15
9	SEM photographs of Specimen A-08 tested at -50°C	17
10	Load versus crack displacement for fracture experiments at -50°C	18
11	SEM photographs of Specimen A-07 tested at 0°C with the shortest ductile crack extension	20
12	SEM photographs of Specimen A-10 tested at 0°C with the longest ductile crack extension	21

Contents (continued)

13	Load versus crack displacement for fracture experiments at 0°C	22
14	Pseudo J-resistance curve estimated from test data at 0°C	23
15	Load and J versus crack displacement for the fracture experiments at 23°C	24
16	SEM photographs of Specimen B-07 tested at 50°C	26
17	Load versus crack displacement for fracture experiments at 50°C	27
18	J/ σ_0 versus displacement for selected specimens tested at -80°, 0°, 23°, and 50°C	29
19	Comparison of ORNL 1T-CT and SRI CRB fracture data	33
A-1	Temperature dependence of the yield and ultimate strengths for HSSI Weld 72W (0.23% copper) unirradiated	A-4
B-1	Geometry of the rigid plastic deformation of the cracked round bar specimen with eccentric ligament	B-2

List of Tables

1	Fatigue crack characteristics for CRB Tests at -150°C	11
2	Results of CRB fracture experiments at -150°C	12
3	Fatigue-crack characteristics for CRB tests at -80°C	13
4	Results of CRB fracture experiments at -80°C	15
5	Fatigue-crack characteristics for CRB tests at -50°C	16
6	Results of CRB fracture experiments at -50°C	16
7	Fatigue-crack characteristics for CRB tests at 0°C	19
8	Results of CRB fracture experiments at 0°C	22

Contents (continued)

9	Fatigue-crack characteristics for CRB tests at 23°C	23
10	Results of CRB fracture experiments at 23°C	24
11	Fatigue-crack characteristics for CRB tests at 50°C	25
12	Results of CRB fracture experiments at 50°C	28
13	Proportionality constant λ between J and δ_{cr}	30
14	Fracture-toughness data for HSSI weld 72W (0.23% copper) unirradiated obtained With 1T-CT specimens	32
A-1	Chemical compositions of submerged-arc weld HSSI 72W (0.23% copper) unirradiated	A-2
A-2	Tensile properties of HSSI Weld 72W unirradiated	A-3
B-1	Error estimate for two CRB tests at 0°C	B-4

Acknowledgments

The authors would like to thank Dr. E. M. Hackett, U.S. Nuclear Regulatory Commission, for suggesting and encouraging this research and Mr. W. R. Corwin and Drs. D. J. Alexander and R. K. Nanstad, Oak Ridge National Laboratory, for supporting the project and providing material, mechanical properties data, and valuable technical advice. The authors also would like to thank their SRI colleagues Leah Alaura-Malinis, Kristen Watts-Penny, Lee Gerrans, and Joyce Berry, who helped with the preparation of this report.

Preface

The work reported here was performed at the Oak Ridge National Laboratory (ORNL) under the Heavy-Section Steel Irradiation (HSSI) Program, W. R. Corwin, Program Manager. The program is sponsored by the Office of Nuclear Regulatory Research of the U.S. Nuclear Regulatory Commission (NRC). The technical monitor for the NRC is M. G. Vassilaros.

This report is designated HSSI Report 12. Reports in this series are listed below:

1. F. M. Haggag, W. R. Corwin, and R. K. Nanstad, Martin Marietta Energy Systems, Inc., Oak Ridge Natl. Lab., Oak Ridge, Tenn., *Irradiation Effects on Strength and Toughness of Three-Wire Series-Arc Stainless Steel Weld Overlay Cladding*, USNRC Report NUREG/CR-5511 (ORNL/TM-11439), February 1990.
2. L. F. Miller, C. A. Baldwin, F. W. Stallman, and F. B. K. Kam, Martin Marietta Energy Systems, Inc., Oak Ridge Natl. Lab., Oak Ridge, Tenn., *Neutron Exposure Parameters for the Metallurgical Test Specimens in the Sixth Heavy-Section Steel Irradiation Series*, USNRC Report NUREG/CR-5409 (ORNL/TM-11267), March 1990.
3. S. K. Iskander, W. R. Corwin, and R. K. Nanstad, Martin Marietta Energy Systems, Inc., Oak Ridge Natl. Lab., Oak Ridge, Tenn., *Results of Crack-Arrest Tests on Two Irradiated High-Copper Welds*, USNRC Report NUREG/CR-5584 (ORNL/TM-11575), December 1990.
4. R. K. Nanstad and R. G. Berggren, Martin Marietta Energy Systems, Inc., Oak Ridge Natl. Lab., Oak Ridge, Tenn., *Irradiation Effects on Charpy Impact and Tensile Properties of Low Upper-Shelf Welds, HSSI Series 2 and 3*, USNRC Report NUREG/CR-5696 (ORNL/TM-11804), August 1991.
5. R. E. Stoller, Martin Marietta Energy Systems, Inc., Oak Ridge Natl. Lab., Oak Ridge, Tenn., *Modeling the Influence of Irradiation Temperature and Displacement Rate on Radiation-Induced Hardening in Ferritic Steels*, USNRC Report NUREG/CR5859 (ORNL/TM-12073), August 1992.
6. R. K. Nanstad, D. E. McCabe, and R. L. Swain, Martin Marietta Energy Systems, Inc., Oak Ridge Natl. Lab., Oak Ridge, Tenn., *Chemical Composition RT_{NDT} Determinations for Midland Weld WF-70*, USNRC Report NUREG/CR-5914 (ORNL-6740), December 1992.
7. R. K. Nanstad, F. M. Haggag, D. E. McCabe, S. K. Iskander, K. O. Bowman, and B. H. Menke, Martin Marietta Energy Systems, Inc., Oak Ridge Natl. Lab., Oak Ridge, Tenn., *Irradiation Effects on Fracture Toughness of Two High-Copper Submerged-Arc Welds*, USNRC Report NUREG/CR-5913 (ORNL/TM-12156/V1), October 1992.

8. S. K. Iskander, W. R. Corwin, and R. K. Nanstad, Martin Marietta Energy Systems, Inc., Oak Ridge Natl. Lab., Oak Ridge, Tenn., *Crack-Arrest Tests on Two Irradiated High-Copper Welds*, USNRC Report NUREG/CR-6139 (ORNL/TM-12513), March 1994.
9. R. E. Stoller, Martin Marietta Energy Systems, Inc., Oak Ridge Natl. Lab., Oak Ridge, Tenn., *A Comparison of the Relative Importance of Copper Precipitates and Point Defects in Reactor Pressure Vessel Embrittlement*, USNRC Report NUREG/CR-6231 (ORNL/TM-6811), December 1994.
10. D. E. McCabe, R. K. Nanstad, S. K. Iskander, and R. L. Swain, Martin Marietta Energy Systems, Inc., Oak Ridge Natl. Lab., Oak Ridge, Tenn., *Unirradiated Material Properties of Midland Weld WF-70*, USNRC Report NUREG/CR-6249 (ORNL/TM-12777), October 1994.
11. P. M. Rice and R. E. Stoller, Lockheed Martin Energy Systems, Oak Ridge Natl. Lab., Oak Ridge, Tenn., *Microstructural Characterization of Selected AEA/UCSB Model FeCuMn Alloys*, USNRC Report NUREG/CR-6332 (ORNL/TM-12980), June 1996.
12. This report.

The HSSI Program includes both follow-on and the direct continuation of work that was performed under the Heavy-Section Steel Technology (HSST) Program. Previous HSST reports related to irradiation effects in pressure vessel materials and those containing unirradiated properties of materials used in HSSI and HSST irradiation programs are tabulated below as a convenience to the reader.

C. E. Childress, Union Carbide Corp. Nuclear Div., Oak Ridge Natl. Lab., Oak Ridge, Tenn., *Fabrication History of the First Two 12-in.-Thick A-533 Grade B, Class 1 Steel Plates of the Heavy-Section Steel Technology Program*, ORNL-4313, February 1969.

T. R. Mager and F. O. Thomas, Westinghouse Electric Corporation, PWR Systems Division, Pittsburgh, Pa., *Evaluation by Linear Elastic Fracture Mechanics of Radiation Damage to Pressure Vessel Steels*, WCAP-7328 (Rev.), October 1969.

P. N. Randall, TRW Systems Group, Redondo Beach, Calif., *Gross Strain Measure of Fracture Toughness of Steels*, HSSTP-TR-3, Nov. 1, 1969.

L. W. Loechel, Martin Marietta Corporation, Denver, Colo., *The Effect of Testing Variables on the Transition Temperature in Steel*, MCR-69-189, Nov. 20, 1969.

W. O. Shabbits, W. H. Pryle, and E. T. Wessel, Westinghouse Electric Corporation, PWR Systems Division, Pittsburgh, Pa., *Heavy-Section Fracture Toughness Properties of A533 Grade B Class 1 Steel Plate and Submerged Arc Weldment*, WCAP-7414, December 1969.

C. E. Childress, Union Carbide Corp. Nuclear Div., Oak Ridge Natl. Lab., Oak Ridge, Tenn., *Fabrication History of the Third and Fourth ASTM A-533 Steel Plates of the Heavy-Section Steel Technology Program*, ORNL-4313-2, February 1970.

P. B. Crosley and E. J. Ripling, Materials Research Laboratory, Inc., Glenwood, Ill., *Crack Arrest Fracture Toughness of A533 Grade B Class 1 Pressure Vessel Steel*, HSSTP-TR-8, March 1970.

F. J. Loss, Naval Research Laboratory, Washington, D.C., *Dynamic Tear Test Investigations of the Fracture Toughness of Thick-Section Steel*, NRL-7056, May 14, 1970.

T. R. Mager, Westinghouse Electric Corporation, PWR Systems Division, Pittsburgh, Pa., *Post-Irradiation Testing of 2T Compact Tension Specimens*, WCAP-7561, August 1970.

F. J. Witt and R. G. Berggren, Union Carbide Corp. Nuclear Div., Oak Ridge Natl. Lab., Oak Ridge, Tenn., *Size Effects and Energy Disposition in Impact Specimen Testing of ASTM A533 Grade B Steel*, ORNL/TM-3030, August 1970.

D. A. Canonico, Union Carbide Corp. Nuclear Div., Oak Ridge Natl. Lab., Oak Ridge, Tenn., *Transition Temperature Considerations for Thick-Wall Nuclear Pressure Vessels*, ORNL/TM-3114, October 1970.

T. R. Mager, Westinghouse Electric Corporation, PWR Systems Division, Pittsburgh, Pa., *Fracture Toughness Characterization Study of A533, Grade B, Class 1 Steel*, WCAP-7578, October 1970.

W. O. Shabbits, Westinghouse Electric Corporation, PWR Systems Division, Pittsburgh, Pa., *Dynamic Fracture Toughness Properties of Heavy-Section A533 Grade B Class 1 Steel Plate*, WCAP-7623, December 1970.

C. E. Childress, Union Carbide Corp. Nuclear Div., Oak Ridge Natl. Lab., Oak Ridge, Tenn., *Fabrication Procedures and Acceptance Data for ASTM A-533 Welds and a 10-in.-Thick ASTM A-543 Plate of the Heavy Section Steel Technology Program*, ORNL-TM-4313-3, January 1971.

D. A. Canonico and R. G. Berggren, Union Carbide Corp. Nuclear Div., Oak Ridge Natl. Lab., Oak Ridge, Tenn., *Tensile and Impact Properties of Thick-Section Plate and Weldments*, ORNL/TM-3211, January 1971.

C. W. Hunter and J. A. Williams, Hanford Eng. Dev. Lab., Richland, Wash., *Fracture and Tensile Behavior of Neutron-Irradiated A533-B Pressure Vessel Steel*, HEDL-TME-71-76, Feb. 6, 1971.

C. E. Childress, Union Carbide Corp. Nuclear Div., Oak Ridge Natl. Lab., Oak Ridge, Tenn., *Manual for ASTM A533 Grade B Class 1 Steel (HSST Plate 03) Provided to the International Atomic Energy Agency*, ORNL/TM-3193, March 1971.

P. N. Randall, TRW Systems Group, Redondo Beach, Calif., *Gross Strain Crack Tolerance of A533-B Steel*, HSSTP-TR-14, May 1, 1971.

C. L. Segaser, Union Carbide Corp. Nuclear Div., Oak Ridge Natl. Lab., Oak Ridge, Tenn., *Feasibility Study, Irradiation of Heavy-Section Steel Specimens in the South Test Facility of the Oak Ridge Research Reactor*, ORNL/TM-3234, May 1971.

H. T. Corten and R. H. Sailors, University of Illinois, Urbana, Ill., *Relationship Between Material Fracture Toughness Using Fracture Mechanics and Transition Temperature Tests*, T&AM Report 346, Aug. 1, 1971.

L. A. James and J. A. Williams, Hanford Eng. Dev. Lab., Richland, Wash., *Heavy Section Steel Technology Program Technical Report No. 21, The Effect of Temperature and Neutron Irradiation Upon the Fatigue-Crack Propagation Behavior of ASTM A533 Grade B, Class 1 Steel*, HEDL-TME 72-132, September 1972.

P. B. Crosley and E. J. Ripling, Materials Research Laboratory, Inc., Glenwood, Ill., *Crack Arrest in an Increasing K-Field*, HSSTP-TR-27, January 1973.

W. J. Stelzman and R. G. Berggren, Union Carbide Corp. Nuclear Div., Oak Ridge Natl. Lab., Oak Ridge, Tenn., *Radiation Strengthening and Embrittlement in Heavy-Section Steel Plates and Welds*, ORNL-4871, June 1973.

J. M. Steichen and J. A. Williams, Hanford Eng. Dev. Lab., Richland, Wash., *High Strain Rate Tensile Properties of Irradiated ASTM A533 Grade B Class 1 Pressure Vessel Steel*, HEDL-TME 73-74, July 1973.

J. A. Williams, Hanford Eng. Dev. Lab., Richland, Wash., *The Irradiation and Temperature Dependence of Tensile and Fracture Properties of ASTM A533, Grade B, Class 1 Steel Plate and Weldment*, HEDL-TME 73-75, August 1973.

J. A. Williams, Hanford Eng. Dev. Lab., Richland, Wash., *Some Comments Related to the Effect of Rate on the Fracture Toughness of Irradiated ASTM A533-B Steel Based on Yield Strength Behavior*, HEDL-SA 797, December 1974.

J. A. Williams, Hanford Eng. Dev. Lab., Richland, Wash., *The Irradiated Fracture Toughness of ASTM A533, Grade B, Class 1 Steel Measured with a Four-Inch-Thick Compact Tension Specimen*, HEDL-TME 75-10, January 1975.

J. G. Merkle, G. D. Whitman, and R. H. Bryan, Union Carbide Corp. Nuclear Div., Oak Ridge Natl. Lab., Oak Ridge, Tenn., *An Evaluation of the HSST Program Intermediate Pressure Vessel Tests in Terms of Light-Water-Reactor Pressure Vessel Safety*, ORNL/TM-5090, November 1975.

- J. A. Davidson, L. J. Ceschini, R. P. Shogan, and G. V. Rao, Westinghouse Electric Corporation, Pittsburgh, Pa., *The Irradiated Dynamic Fracture Toughness of ASTM A533, Grade B, Class 1 Steel Plate and Submerged Arc Weldment*, WCAP-8775, October 1976.
- J. A. Williams, Hanford Eng. Dev. Lab., Richland, Wash., *Tensile Properties of Irradiated and Unirradiated Welds of A533 Steel Plate and A508 Forgings*, NUREG/CR-1158 (ORNL/SUB-79/50917/2), July 1979.
- J. A. Williams, Hanford Eng. Dev. Lab., Richland, Wash., *The Ductile Fracture Toughness of Heavy-Section Steel Plate*, NUREG/CR-0859, September 1979.
- K. W. Carlson and J. A. Williams, Hanford Eng. Dev. Lab., Richland, Wash., *The Effect of Crack Length and Side Grooves on the Ductile Fracture Toughness Properties of ASTM A533 Steel*, NUREG/CR-1171 (ORNL/SUB-79/50917/3), October 1979.
- G. A. Clarke, Westinghouse Electric Corp., Pittsburgh, Pa., *An Evaluation of the Unloading Compliance Procedure for J-Integral Testing in the Hot Cell, Final Report*, NUREG/CR-1070 (ORNL/SUB-7394/1), October 1979.
- P. B. Crosley and E. J. Ripling, Materials Research Laboratory, Inc., Glenwood, Ill., *Development of a Standard Test for Measuring K_{Ic} with a Modified Compact Specimen*, NUREG/CR-2294 (ORNL/SUB-81/7755/1), August 1981.
- H. A. Domian, Babcock and Wilcox Company, Alliance, Ohio, *Vessel V-8 Repair and Preparation of Low Upper-Shelf Weldment*, NUREG/CR-2676 (ORNL/SUB/81-85813/1), June 1982.
- R. D. Cheverton, S. K. Iskander, and D. G. Ball, Union Carbide Corp. Nuclear Div., Oak Ridge Natl. Lab., Oak Ridge, Tenn., *PWR Pressure Vessel Integrity During Overcooling Accidents: A Parametric Analysis*, NUREG/CR-2895 (ORNL/TM-7931), February 1983.
- J. G. Merkle, Union Carbide Corp. Nuclear Div., Oak Ridge Natl. Lab., Oak Ridge, Tenn., *An Examination of the Size Effects and Data Scatter Observed in Small Specimen Cleavage Fracture Toughness Testing*, NUREG/CR-3672 (ORNL/TM-9088), April 1984.
- W. R. Corwin, Martin Marietta Energy Systems, Inc., Oak Ridge Natl. Lab., Oak Ridge, Tenn., *Assessment of Radiation Effects Relating to Reactor Pressure Vessel Cladding*, NUREG/CR-3671 (ORNL-6047), July 1984.
- W. R. Corwin, R. G. Berggren, and R. K. Nanstad, Martin Marietta Energy Systems, Inc., Oak Ridge Natl. Lab., Oak Ridge, Tenn., *Charpy Toughness and Tensile Properties of a Neutron Irradiated Stainless Steel Submerged-Arc Weld Cladding Overlay*, NUREG/CR-3927 (ORNL/TM-9709), September 1984.

J. J. McGowan, Martin Marietta Energy Systems, Inc., Oak Ridge Natl. Lab., Oak Ridge, Tenn., *Tensile Properties of Irradiated Nuclear Grade Pressure Vessel Plate and Welds for the Fourth HSST Irradiation Series*, NUREG/CR-3978 (ORNL/TM-9516), January 1985.

J. J. McGowan, Martin Marietta Energy Systems, Inc., Oak Ridge Natl. Lab., Oak Ridge, Tenn., *Tensile Properties of Irradiated Nuclear Grade Pressure Vessel Welds for the Third HSST Irradiation Series*, NUREG/CR-4086 (ORNL/TM-9477), March 1985.

W. R. Corwin, G. C. Robinson, R. K. Nanstad, J. G. Merkle, R. G. Berggren, G. M. Goodwin, R. L. Swain, and

T. D. Owings, Martin Marietta Energy Systems, Inc., Oak Ridge Natl. Lab., Oak Ridge, Tenn., *Effects of Stainless Steel Weld Overlay Cladding on the Structural Integrity of Flawed Steel Plates in Bending, Series 1*, NUREG/CR-4015 (ORNL/TM-9390), April 1985.

W. J. Stelzman, R. G. Berggren, and T. N. Jones, Martin Marietta Energy Systems, Inc., Oak Ridge Natl. Lab.,
Oak Ridge, Tenn., *ORNL Characterization of Heavy-Section Steel Technology Program Plates 01, 02, and 03*, NUREG/CR-4092 (ORNL/TM-9491), April 1985.

G. D. Whitman, Martin Marietta Energy Systems, Inc., Oak Ridge Natl. Lab., Oak Ridge, Tenn., *Historical Summary of the Heavy-Section Steel Technology Program and Some Related Activities in Light-Water Reactor Pressure Vessel Safety Research*, NUREG/CR-4489 (ORNL-6259), March 1986.

R. H. Bryan, B. R. Bass, S. E. Bolt, J. W. Bryson, J. G. Merkle, R. K. Nanstad, and G. C. Robinson, Martin Marietta Energy Systems, Inc., Oak Ridge Natl. Lab., Oak Ridge, Tenn., *Test of 6-in.-Thick Pressure Vessels. Series 3: Intermediate Test Vessel V-8A Ñ Tearing Behavior of Low Upper-Shelf Material*, NUREG-CR-4760 (ORNL-6187), May 1987.

D. B. Barker, R. Chona, W. L. Fournery, and G. R. Irwin, University of Maryland, College Park, Md., *A Report on the Round Robin Program Conducted to Evaluate the Proposed ASTM Standard Test Method for Determining the Plane Strain Crack Arrest Fracture Toughness, K_{Ic} , of Ferritic Materials*, NUREG/CR-4966 (ORNL/SUB/79-7778/4), January 1988.

L. F. Miller, C. A. Baldwin, F. W. Stallman, and F. B. K. Kam, Martin Marietta Energy Systems, Inc., Oak Ridge Natl. Lab., Oak Ridge, Tenn., *Neutron Exposure Parameters for the Metallurgical Test Specimens in the Fifth Heavy-Section Steel Technology Irradiation Series Capsules*, NUREG/CR-5019 (ORNL/TM-10582), March 1988.

J. J. McGowan, R. K. Nanstad, and K. R. Thoms, Martin Marietta Energy Systems, Inc., Oak Ridge Natl. Lab.,
Oak Ridge, Tenn., *Characterization of Irradiated Current-Practice Welds and A533 Grade B Class 1 Plate for Nuclear Pressure Vessel Service*, NUREG/CR-4880 (ORNL-6484/V1 and V2), July 1988.

R. D. Cheverton, W. E. Pennell, G. C. Robinson, and R. K. Nanstad, Martin Marietta Energy Systems, Inc., Oak Ridge Natl. Lab., Oak Ridge, Tenn., *Impact of Radiation Embrittlement on Integrity of Pressure Vessel Supports for Two PWR Plants*, NUREG/CR-5320 (ORNL/TM-10966), February 1989.

J. G. Merkle, Martin Marietta Energy Systems, Inc., Oak Ridge Natl. Lab., Oak Ridge, Tenn., *An Overview of the Low-Upper-Shelf Toughness Safety Margin Issue*, NUREG/CR-5552 (ORNL/TM-11314), August 1990.

R. D. Cheverton, T. L. Dickson, J. G. Merkle, and R. K. Nanstad, Martin Marietta Energy Systems, Inc., Oak Ridge Natl. Lab., Oak Ridge, Tenn., *Review of Reactor Pressure Vessel Evaluation Report for Yankee Rowe Nuclear Power Station (YAEC No. 1735)*, NUREG/CR-5799 (ORNL/TM-11982), March 1992.

1. Introduction

Evaluation of the structural integrity of nuclear power plants depends, in many cases, on the ability to measure the fracture resistance of irradiated structural materials. Most irradiation surveillance specimens are small, of a size comparable to that of Charpy specimens. Unfortunately, Charpy specimens do not provide fracture-resistance data that can be directly used in fracture-mechanics analyses. Therefore, the nuclear power community has a critical need for reliable small-specimen test methods for characterizing the fracture properties of nuclear power plant materials. To address this need, SRI conducted a research program aimed at demonstrating the feasibility of using small fatigue-precracked round bars to reliably measure the initiation fracture toughness of ductile, nuclear pressure vessel steels and weldments.

Earlier work by several authors indicated that cracked round bars (CRBs) present several advantages for fracture-toughness testing in the elastic, elastic-plastic, and fully plastic regimes.¹⁻⁷ In particular, a high degree of constraint may be achieved at the tip of the crack under fully plastic conditions, even when the cross section of the uncracked ligament is small.⁷ Therefore, CRBs offer the possibility of using small specimens, comparable in size to Charpy specimens, to estimate toughness parameters under conditions representative of conditions at the tips of cracks in large, thick components. Another advantage associated with the small size of CRBs is that they can be loaded at high loading rates with relative ease.⁸⁻¹⁰ Finally, the circular symmetry of the specimen greatly simplifies numerical simulations of experiments to evaluate the stress and strain fields in the specimen.

In our project, we tested a weldment material for which fracture-toughness data had been previously obtained at several temperatures by Oak Ridge National Laboratory (ORNL) using 1T-compact tension (CT) specimens. To demonstrate the usefulness of the CRB test, we measured toughness values with CRBs at six temperatures (-150° , -80° , -50° , 0° , 23° , and 50°C) and compared the results with the 1T-CT data obtained by ORNL. A secondary focus of our study was to identify problems associated with the testing and data-reduction methods used with the CRB specimens and, when possible within the limited scope of the project, to solve these problems.

2. Experimental Procedure

2.1 Material

We tested a weldment, Heavy-Section Steel Irradiation (HSSI) Weld 72W (0.23% copper) unirradiated, produced by submerged arc-welding and joining of 218-mm (8.6-in.)-thick A533 grade B class 2 pressure vessel steel plates. We received the material from ORNL in the form of blanks roughly $19 \times 19 \times 102$ mm ($0.75 \times 0.75 \times 4.25$ in.) cut from three 254-mm (10-in.)-wide by 20-mm (0.79 in.)-thick slabs containing the weld. The weld itself was approximately 30 mm (1.18 in.) wide with its axis oriented along the 254-mm (10-in.) width of the slabs. Ten specimen blanks were cut along the width of each slab and were numbered A-01 through A-10, B-01 through B-10, and C-01 through C-10, respectively. The longitudinal axis of the blanks was normal to the thickness and width directions and was therefore normal to the midplane of the weld. The position of the weld midplane was scribed on each of the blanks and corresponded to the midplane of the blank.

The chemical composition and mechanical properties of the parent HSSI Weld 72W, as determined and supplied by ORNL, are given in Appendix A. We assume that the weldment we tested has the same composition and mechanical properties.

2.2 Specimen Geometry and Precracking Procedure

Figure 1 shows the geometry and dimensions of the round bars used in our fracture experiments. The outside radius of the bar R_0 is 16 mm (0.625 in.), the initial notch radius r_n is 8 mm (0.314 in.), and the gage length over which axial displacements are measured during the experiments is 50.8 mm (2 in.). We machined the notch in the CRBs so that the minimum cross section is coincident with the midplane of the weldment.

Annular cracks that are concentric with the round cross section of tensile bars can be initiated and grown by rotating fatigue. To achieve this loading mode, we modified a commercial lathe so that a round bar mounted between centers can be loaded in four-point bending. Figure 2 illustrates the fatiguing arrangement. Two self-aligning ball bearings attached to a loading frame, which can move vertically, apply a bending moment to the reduced section of the notched bar. A load cell mounted above the loading frame measures the load applied to the specimen. An optical sensor aimed at the chuck of the lathe is connected to an impulse counter to track the number of loading cycles applied to the specimen.

At the onset of fatiguing, we select the load to achieve a desired stress intensity range and apply this load to the specimen by tightening a nut and moving the loading frame upward (fixed displacement loading conditions). We applied a load of approximately 1000 N, which corresponds to a stress intensity factor range of approximately $\pm 17.3 \text{ MPa}\sqrt{\text{m}}$ (for the notched but uncracked specimen) to $25 \text{ MPa}\sqrt{\text{m}}$ [for a ratio of crack length to specimen radius (a/R_0) of 0.6]. We used the linear-elastic handbook solution of Reference 11 to estimate the stress intensity factor during rotating fatigue precracking. After preloading

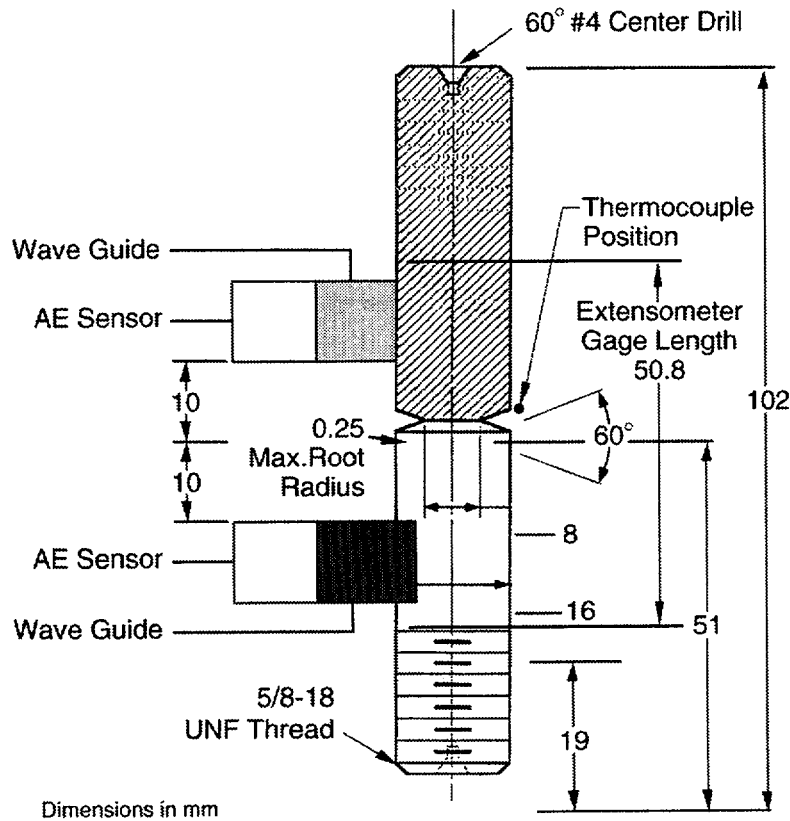
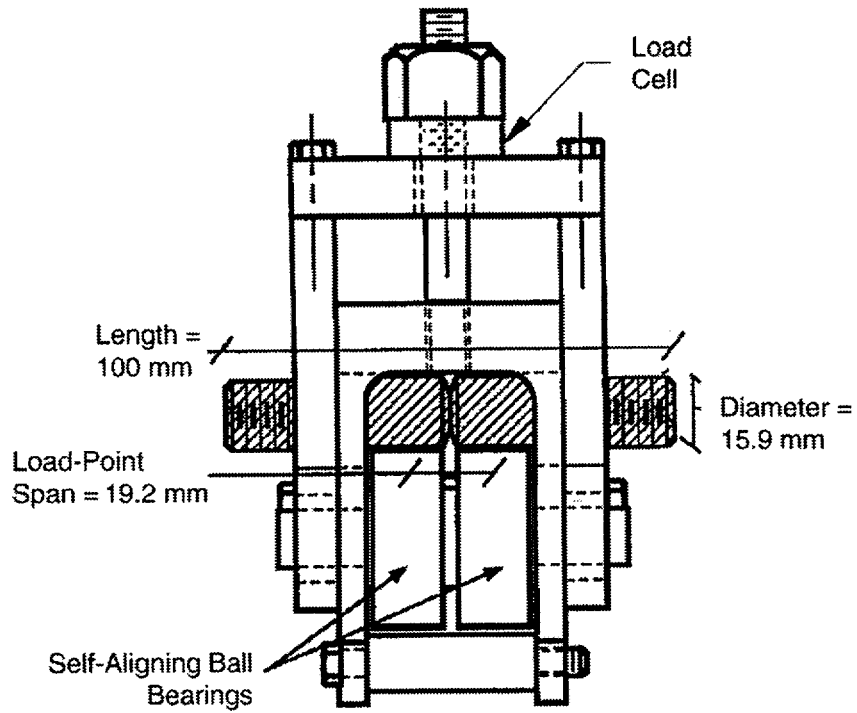


Figure 1. Geometry and dimensions of notched round bar specimen.

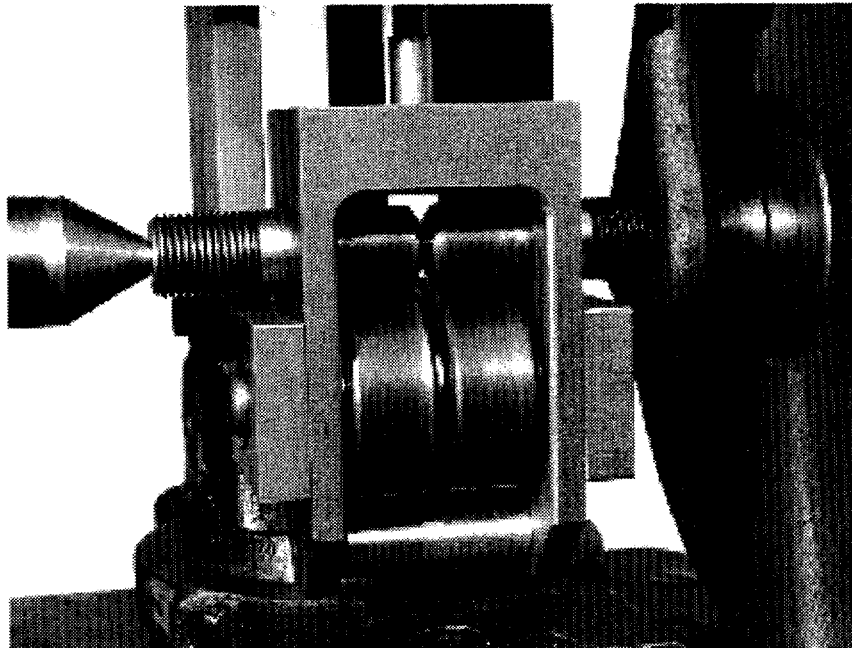
the specimen, we started the lathe at a rotating speed of 900 rpm. As the fatigue crack initiates and propagates around the specimen, the bending load drops. However, monitoring the bending load did not provide an accurate enough indication of fatigue crack growth because some of the observed load relaxation was associated with fretting damage to the specimen at points of contact with the centers and the roller bearings.

Therefore, to evaluate the fatigue crack length, we removed the specimen from the lathe after 25,000 fatiguing cycles and measured its stiffness under pure tensile loading. We applied loads well in the elastic range and not exceeding 25% of the maximum load during the fracture test. The change in stiffness, together with the experimentally measured stiffness versus uncracked ligament radius curve shown in Figure 3, allowed us to monitor fatigue crack growth quite accurately.* If the estimated value of a/R_0 was smaller than the desired 0.60 value, we applied an additional 10,000 cycles of rotating fatigue and repeated the stiffness measurement. In this way, after an initial learning phase, we were able to introduce well-controlled annular fatigue cracks with essentially circular uncracked ligaments in most

* A curve fit of the data in Figure 3 provides the following relationship between stiffness S (in MNm^{-1}) and ligament radius r_0 (in millimeters): $S = -0.459 + 204.7 r_0 - 12.721 r_0^2$.



(a) Four-point-bend loading arrangement.



(b) Actual facility.

Figure 2. Rotating fatigue precracking facility.

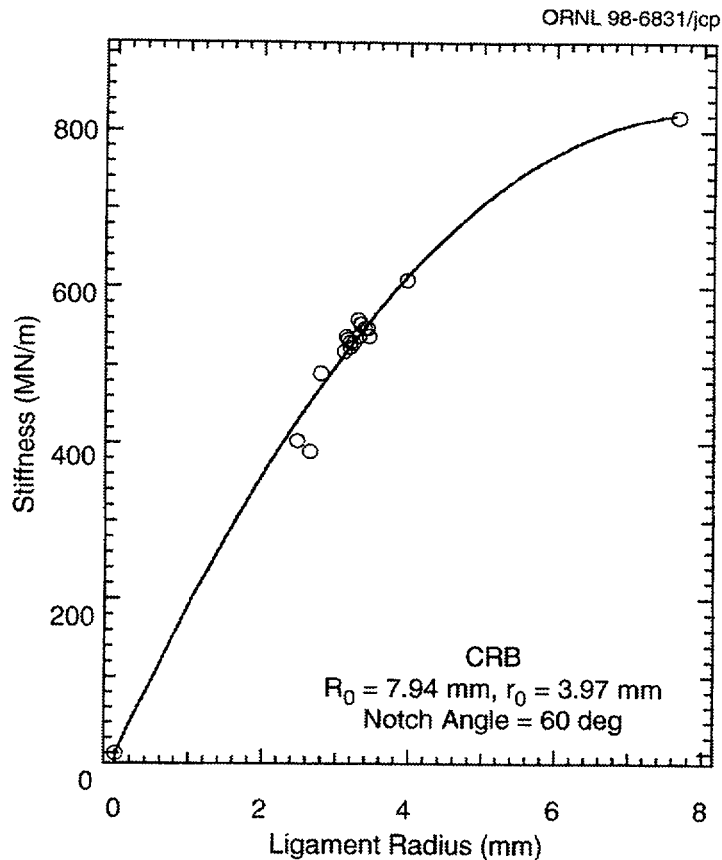


Figure 3. Stiffness versus uncracked ligament radius for the cracked round bar specimen of Figure 1 under tensile loading.

CRBs. We defined the eccentricity of the circular uncracked ligament as the distance between its center and the specimen center line. The eccentricity of the remaining ligament may have several causes, such as misalignment in the precracking fixture, residual stresses in the weldment, or an inhomogeneous microstructure. Eccentricity is an undesirable feature because it introduces a bending component to the crack tip loading during the experiment. We established that if the fatigue crack depth does not exceed about 1 mm (0.039 in.), we can keep ligament eccentricity small and at an acceptable value.

We fabricated a total of 30 CRB specimens and precracked 26 of them. The resulting crack length (i.e., notch plus fatigue crack) ranged from 4.49 to 5.54 mm (0.18 to 0.22 in.), corresponding to ratios of crack depth to specimen radius of 0.56 to 0.70. Eccentricities ranged from 0.04 to 0.62 mm (0.002 to 0.024 in.).

2.3 Fracture Test Procedure

We performed a total of 26 fracture experiments: four each at -150° , -50° , and 0°C ; seven tests at -80°C ; one test at 23°C ; and six tests at 50°C . We fractured the precracked specimens under machine

ram displacement control, in a servohydraulic, universal-testing machine using a loading arrangement similar to the arrangement for a standard tensile test. Figure 4 shows the experimental setup for tests at -150° , -80° , -50° , and 0°C . The specimen and most of the test instrumentation were enclosed in an insulating chamber made of polymer foam. A set of hollow clevises through which we circulated liquid nitrogen served to cool the specimen by conduction. In addition, we bubbled liquid nitrogen directly into the chamber to provide additional cooling and to stabilize the temperature. We used a similar arrangement for tests at 50°C , except that we removed the cooling clevises and wrapped heating tape around the loading train to heat the specimen by conduction. The long loading train provided for a rather high machine compliance, which promoted instability after maximum load, even under displacement control.

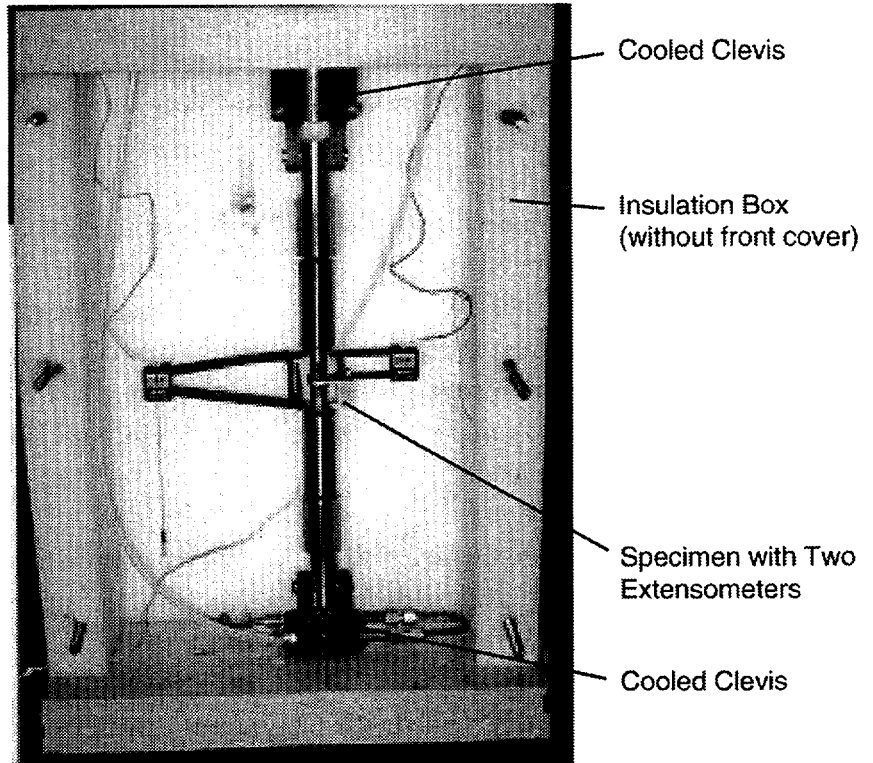


Figure 4. Experimental arrangement for fracture experiments at temperatures below room temperature.

Figure 1 shows the placement of the instrumentation on the CRB specimen. We placed two 50.8-mm (2-in.) extensometers at 180 degrees to each other and symmetrically straddling the crack plane. We used two extensometers to establish the amount of bending occurring during the experiment. Before the experiment, we performed several partial loadings of the specimen (to no more than 25% of the peak load), while incrementally rotating the pair of extensometers around the circumference after each loading cycle to establish the direction of maximum bending (and the direction of the neutral axis). We then marked these directions on the specimen, without removing it from the test setup.

We measured the specimen temperature with one thermocouple placed just above the notch and held in close contact with the steel surface by a steel strap. For the experiments at 0°C and the selected experiment at 50°C , we also mounted two acoustic emission (AE) sensors* on the specimen by means of two aluminum wave guides. We placed the sensors symmetrically, one on each side of the crack plane and about 20 mm (0.79 in.) apart. The AE data served to identify the onset of crack extension for tests in

* Physical Acoustics Corporation PAC Locan 320 System with model R15 sensors. The output signal of the sensors was preamplified by 40 dB and then amplified an additional 30 dB by the Locan 320 System.

which stable ductile crack growth preceded unstable ductile or cleavage fracture. We measured the load applied to the specimen with the load cell of the testing system.

The digital acquisition equipment of the servohydraulic machine (MTS Teststar System) and the AE system recorded the test data.

After orienting the two extensometers along the direction of maximum bending, we cooled (or heated) the specimen to slightly below (or above) the desired test temperature. We then let the specimen temperature drift and stabilize within a $\pm 1^\circ\text{C}$ band around the nominal temperature. At this point, we started loading the specimen at a ram displacement rate of 0.25 mm/min while we continuously monitored the temperature history on a strip chart recorder. With this procedure, we were able to maintain the specified test temperatures to within $\pm 1^\circ\text{C}$ for all experiments. For all but selected experiments at 50°C , we loaded the specimens continuously up to complete, unstable fracture. As discussed in the following, we could not record meaningful AE signals in the tests at 50°C , although observations of the fracture surface revealed extensive ductile tear. To establish whether this tear occurred before instability or even before peak load, we performed tests on three specimens in which we interrupted loading after different amounts of deformation but before instability. We unloaded the specimens, heat-tinted them, and broke them open to inspect for evidence of ductile tear at the point where we interrupted the test. During the tests at 50°C with two additional specimens, we performed partial unloadings at regular deformation intervals to establish whether the unloading compliance method could serve to monitor crack initiation and extension.

2.4 Fractographic Observations

After each fracture test, we measured the dimensions and characterized the geometry of the specimen's uncracked ligament using an optical microscope at 10 to 40 power. We established the amount of crack extension by ductile tearing and the crack depth at the transition between ductile and cleavage fracture when we could distinguish them clearly. We also observed the fracture surface of selected specimens in the scanning electron microscope (SEM) to establish the microscopic mode of fracture. For cases where cleavage dominated, we determined whether cleavage was associated with any prior ductile tearing in the region of the blunted, initial fatigue crack tip.

2.5 Data Reduction

2.5.1 Displacement Measurements

As indicated previously, eccentricity of the uncracked ligament can introduce bending in the CRB. We also established that small misalignments in the specimen gripping arrangement can introduce bending. In this feasibility study, short of eliminating these bending sources, we monitored the magnitude of their

effect in all the experiments by means of the extensometers pair. Figure 5 shows examples of load-displacement curves for two experiments with significant and negligible bending, respectively. We obtained all the results presented in this report by using the average of the two extensometer displacements; that is, neglecting the effect of bending. An estimate of the error introduced by using the average displacement and neglecting the bending component of loading indicates that it is less than 10% for most of the cases considered here (see Appendix B).

2.5.2 Fracture Initiation Point

Identifying the point along the load-displacement curve at which (stable or unstable, ductile or cleavage) fracture initiates is essential to obtaining consistent initiation-toughness data. Throughout this study (with the exception of one experiment), we assumed that fracture initiation occurs at maximum load. The evidence obtained from interrupted experiments, from AE data, and from fractographic observations supports this assumption. Peak load and stability analyses presented in Appendix C lend further credibility to the assumption. Therefore, the toughness data presented in this report correspond to peak load values unless stated differently.

2.5.3 Estimation of Fracture Toughness

We calculated toughness values from the experimental data in terms of the J-integral. To estimate J from load-displacement records, we used the expression proposed by Rice et al.¹²

$$J = \frac{1}{(2\pi r_0^2)} \left[3 \int_0^{\delta_{cr}} Pd\delta_{cr} - P\delta_{cr} \right], \quad (1)$$

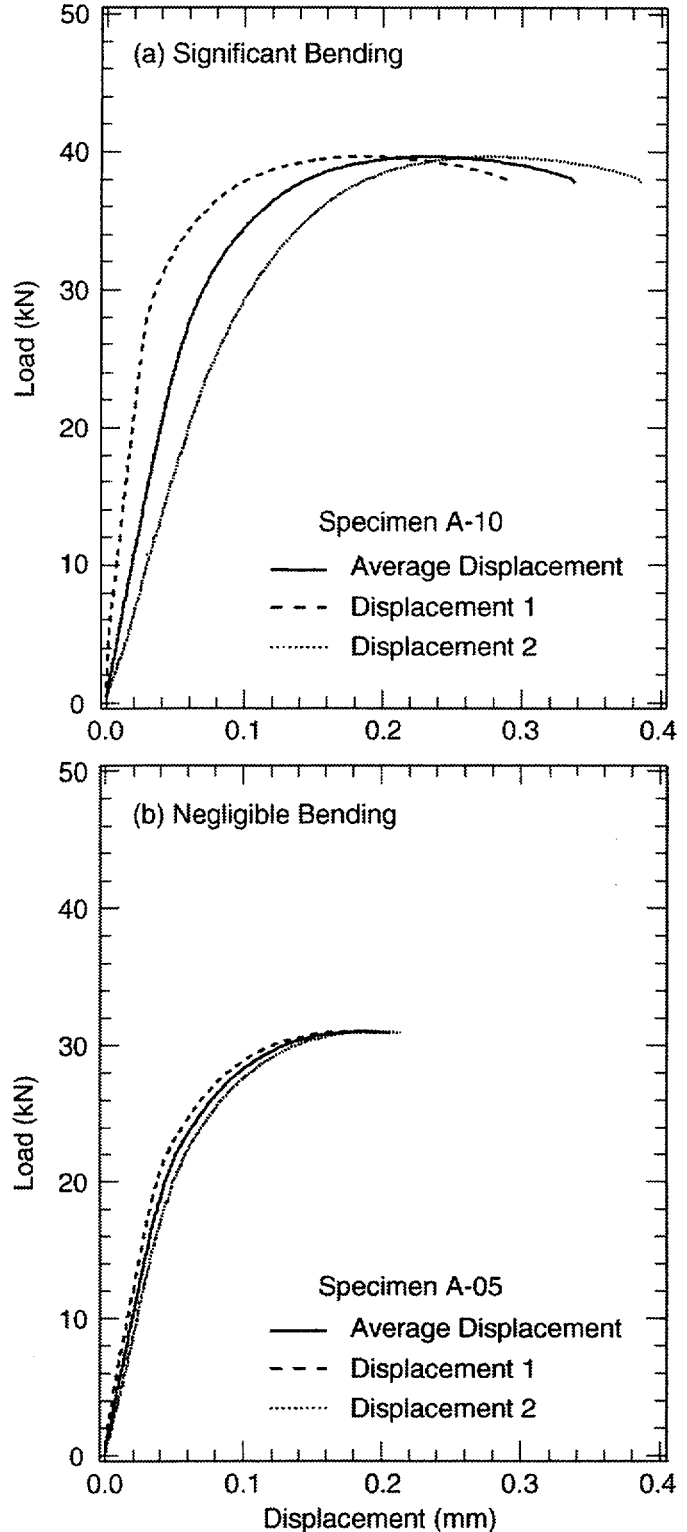


Figure 5. Load versus displacement curves for experiments with loading.

where P is the applied load, δ_{cr} is the load-point displacement caused by the presence of the crack (or crack displacement), and r_0 is the radius of the uncracked ligament.

The load-displacement records produced in our experiments do not yield δ_{cr} directly since we measure the elongation of the specimen between two points separated by 50.8 mm (2.0 in.), as indicated in Figure 1. We estimated δ_{cr} by noting that all the plastic deformation of the specimen is associated with the crack (as indicated by finite-element calculations) and subtracting the elastic contribution of the uncracked specimen δ_{sp} from the total measured displacement.

For a given load P , we obtained the elastic-specimen displacement from the relationship

$$\delta_{sp} = PC_{unscr} \quad , \quad (2)$$

where C_{unscr} is the compliance of the uncracked specimen, that is, of the smooth round bar taken as

$$C_{unscr} = \frac{l_0}{\pi R_0^2 E} \quad . \quad (3)$$

In Equation (3), l_0 is the gage length over which specimen displacements are measured during the experiment, R_0 is the radius of the unnotched region of the specimen, and E is Young's modulus. As mentioned previously, we used the average of the two displacement measurements when evaluating Equation (1).

We convert J values to K values using the customary relation

$$K = \sqrt{\frac{JE}{(1 - \nu^2)}} \quad , \quad (4)$$

with Poisson's ratio ν taken as 0.3 and E as 210 GPa.

We estimated initiation toughness data using Equations (1) through (4) and load-displacement data at maximum load. For the experiments at 0°C, we also estimated a K value at the onset of cleavage (after some amount of ductile tearing) by assuming that all the ductile crack growth observed on the fracture surface occurred in a stable manner before cleavage instability. Therefore, we introduced the radius of the cleavage region (measured on the fracture surface) in lieu of r_0 in Equation (1) and were able to obtain a multiple specimen J -resistance curve for this test temperature.

Finally, the specimens tested at -150°C fractured under essentially linear-elastic or small-scale yielding conditions. For these experiments, we also evaluated the initiation fracture toughness using the linear-elastic expression given in Reference 11.

3. Experimental Results

This section summarizes the results for the six series of tests performed in the feasibility study. For each test temperature, we present the load versus crack-displacement curves and the value of the initiation toughness. For most test temperatures, we also present photographs of the fracture surfaces of selected specimens, identifying the fracture mode and the geometry of the uncracked ligament.

3.1 Tests at -150°C

We tested four specimens at -150°C . Table 1 summarizes the characteristics of the fatigue cracks for these specimens. All four specimens fractured by pure cleavage.

Table 1. Fatigue crack characteristics for CRB tests at -150°C

Specimen no.	Average crack depth (mm)	a/R	Eccentricity (mm)
C-04	4.79	0.60	0.15
C-07	4.67	0.59	0.10
C-08	4.54	0.70	0.62
C-10	4.69	0.59	0.19

Figure 6 shows the load versus crack-displacement curves measured in the tests at -150°C . All specimens broke by unstable crack extension in the rising part of the loading curve with little or no plastic deformation. We estimated the initiation toughness from the curves in Figure 6, using the J analysis and the linear-elastic analysis. Table 2 lists the values we obtained in these experiments. The values range from 45 to 77 $\text{MPa}\sqrt{\text{m}}$ for the toughness obtained with the J analysis (Column 4) and from 48 to 58 $\text{MPa}\sqrt{\text{m}}$ for the toughness obtained with the linear-elastic analysis (Column 5).

3.2 Tests at -80°C

We tested seven specimens at -80°C . Table 3 summarizes the characteristics of the fatigue cracks for these specimens. Figure 7 shows SEM photographs of the fracture surface of Specimen B-04 (the specimen with the second-lowest toughness). Fracture occurs by cleavage over the entire surface except very near the original fatigue-crack front where we observe a narrow band of ductile voids. This region corresponds to the blunted fatigue-crack tip. The ligament of ductile voids probably failed after cleavage-fracture initiation occurred ahead of the original crack tip. Limited fractographic observations on Specimen B-05 (the specimen with the highest toughness) reveal a wider ductile ligament. These

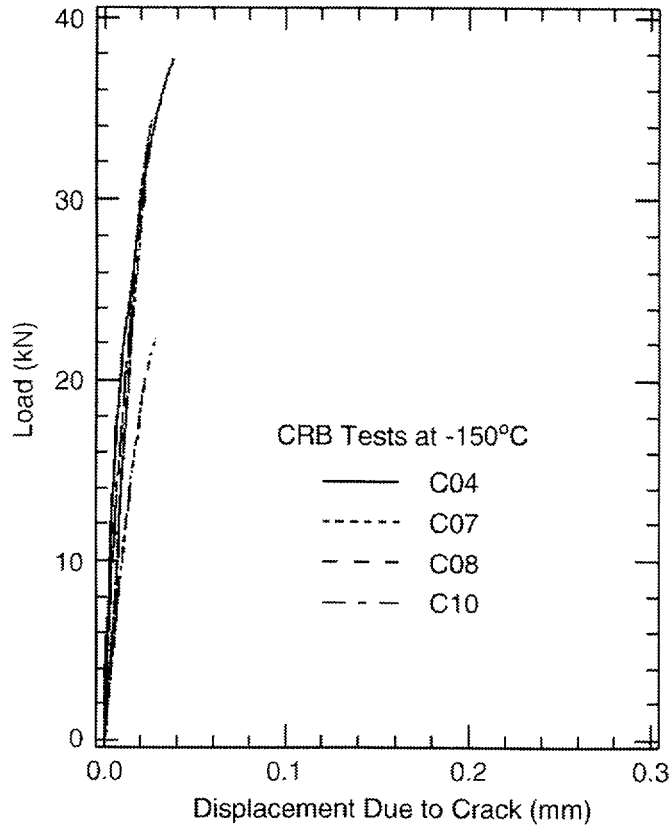


Figure 6. Load versus crack displacement for fracture experiments at -150°C.

Table 2. Results of CRB fracture experiments at -150°C

1	2	3	4	5
Specimen no.	Average radius of uncracked ligament (mm)	J at peak load (kJ/m ²)	K from J of column 3 (MPa√m)	K from linear-elastic analysis, Eq. (MPa√m)
C-04	3.15	26	77	58
C-07	3.27	7	39	50
C-08	2.40	13	55	53
C-10	3.25	9	45	49

**Table 3. Fatigue-crack characteristics for
CRB tests at -80°C**

Specimen no.	Average crack depth (mm)	a/R	Eccentricity (mm)
B-02	4.70	0.59	0.22
B-04	4.64	0.58	0.10
B-05	4.51	0.57	0.08
B-06	4.49	0.56	0.12
C-03	4.63	0.58	0.07
C-06	4.59	0.58	0.10
C-09	4.57	0.58	0.10

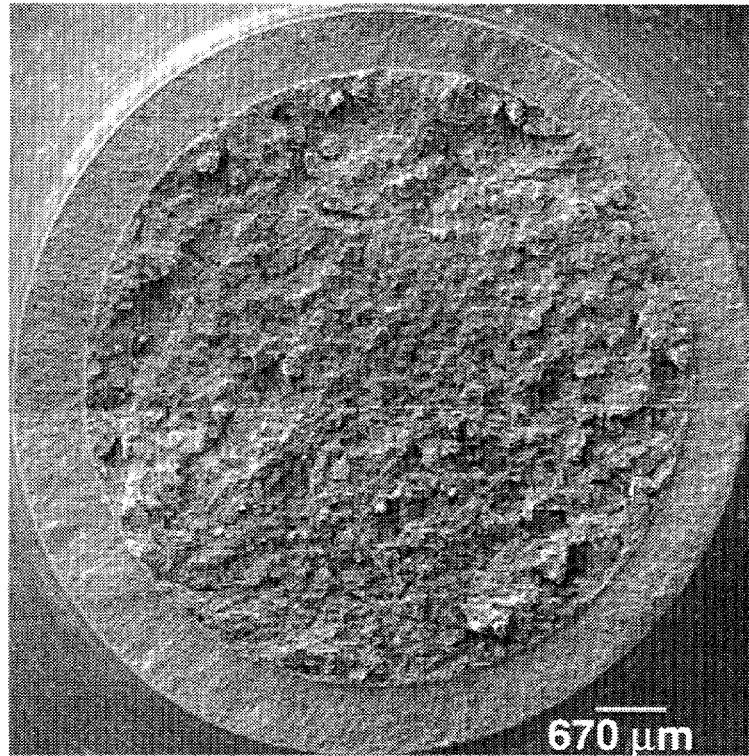
results suggest that the width of the ductile region correlates with the value of the initiation toughness measured with the particular specimen.

Figure 8 shows the load versus crack-displacement curves measured in the tests at -80°C . All specimens broke by unstable crack extension in the rising part of the loading curve. We estimated the initiation toughness from the curves in Figure 8. The values we obtained are listed in Table 4. The experiments yielded K values ranging from 91 to $138 \text{ MPa}\sqrt{\text{m}}$.

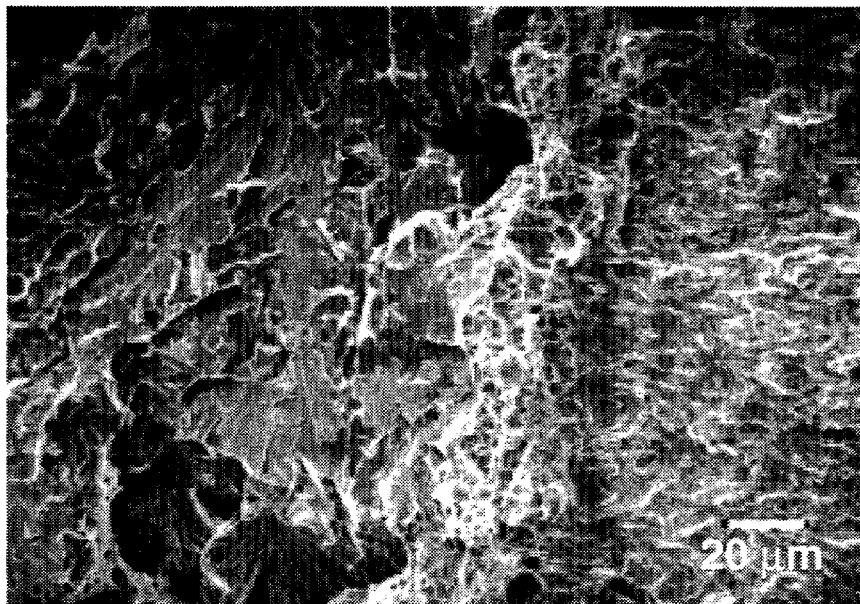
3.3 Tests at -50°C

We tested four specimens at -50°C . Table 5 summarizes the characteristics of the fatigue cracks for these specimens. Figure 9 shows SEM photographs of the fracture surface of Specimen A-08 (the specimen with the lowest toughness) and clearly demonstrates that the specimen fractured by cleavage. We observe only a very narrow ductile ligament along the original fatigue crack tip (Figure 9b) or no ductile ligament at all. In contrast, in Specimen B-01 (the specimen with the highest toughness), the ligament is significantly wider ($\approx 80 \mu\text{m}$), an observation that again suggests a correlation between ductile ligament width and toughness.

Figure 10 shows the load versus crack-displacement curves measured in the tests at -50°C . All specimens broke by unstable crack extension in the rising part of the loading curve. We estimated the initiation toughness from the curves in Figure 10, and the values we obtained are listed in Table 6. The experiments yielded K values ranging from 93 to $166 \text{ MPa}\sqrt{\text{m}}$. The highest value corresponds to Specimen B-01, for which we observed a significantly wider ductile ligament at the initial crack tip.



(a) Overall view of fracture surface.



(b) Region near original fatigue crack tip showing narrow band of ductile voids.

Figure 7. SEM photographs of Specimen B-04 tested at -80°C .

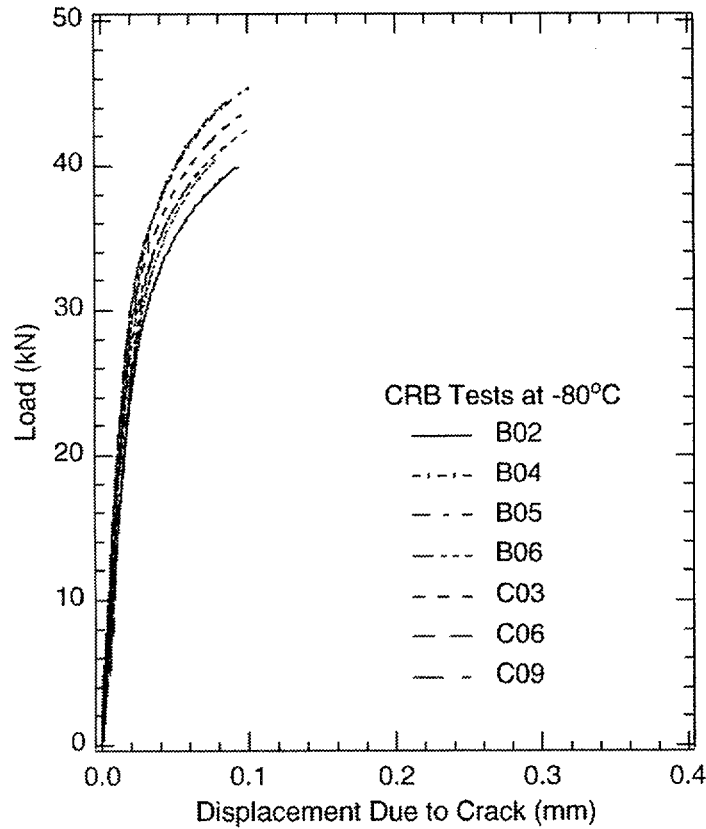


Figure 8. Load versus crack displacement for fracture experiments at -80°C.

Table 4. Results of CRB fracture experiments at -80°C

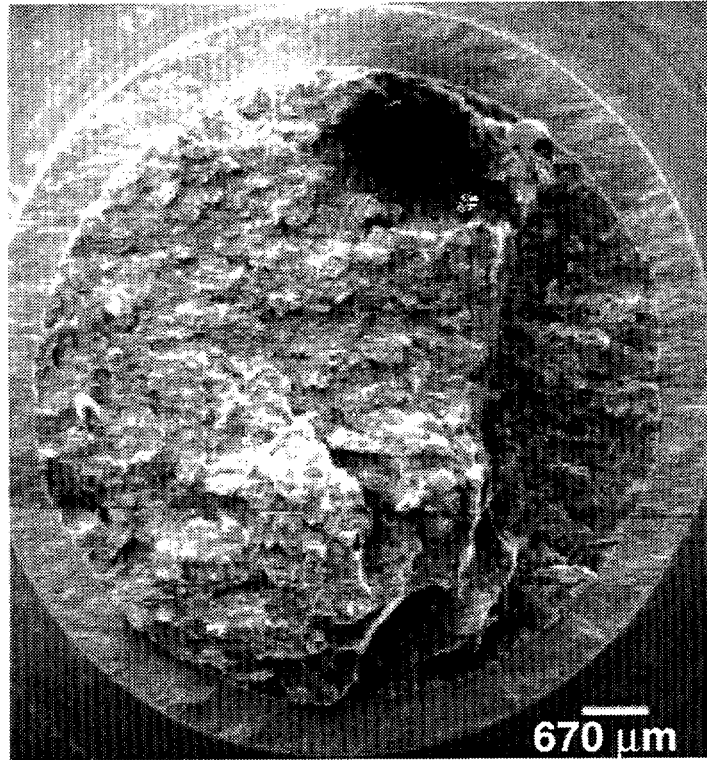
1	2	3	4
Specimen no.	Average radius of uncracked ligament (mm)	J at peak load (kJ/m ²)	K from J of column 3 (MPa√m)
B-02	3.24	72	129
B-04	3.30	55	113
B-05	3.43	82	138
B-06	3.45	67	125
C-03	3.31	82	137
C-06	3.35	79	135
C-09	3.37	36	91

**Table 5. Fatigue-crack characteristics for
CRB tests at -50°C**

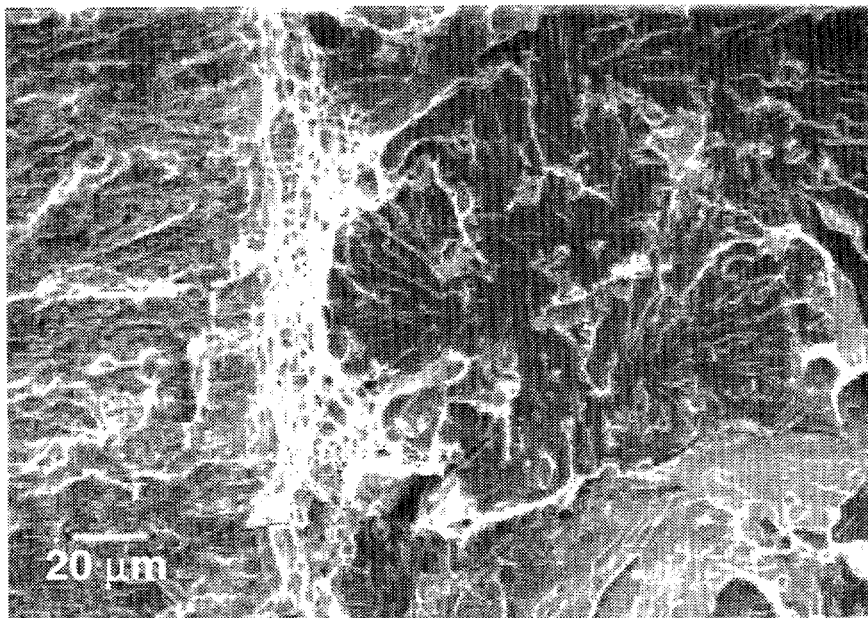
Specimen no.	Average crack depth (mm)	a/R	Eccentricity (mm)
A-08	4.52	0.57	0.04
A-09	4.61	0.58	0.05
B-01	4.60	0.58	0.05
B-03	4.75	0.60	0.29

Table 6. Results of CRB fracture experiments at -50°C

1	2	3	4
Specimen no.	Average radius of uncracked ligament (mm)	J at peak load (kJ/m ²)	K from J of column 3 (MPa√m)
A-08	3.39	38	93
A-09	3.33	55	113
B-01	3.34	119	166
B-03	3.19	38	94



(a) Overall view of fracture surface.



(b) Region near original fatigue crack tip showing narrow band of ductile voids.

Figure 9. SEM photographs of Specimen A-08 tested at -50°C .

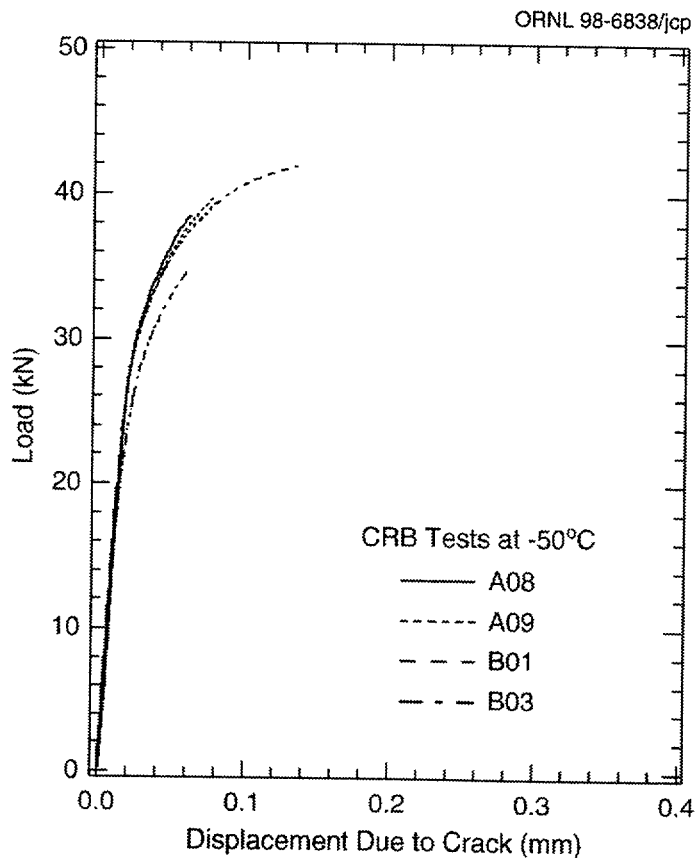


Figure 10. Load versus crack displacement for fracture experiments at -50°C .

3.4 Tests at 0°C

We tested four specimens at 0°C . Table 7 summarizes the characteristics of the fatigue cracks for these specimens. In all experiments, fracture was initiated by ductile tearing and then was propagated by cleavage. The degree of ductile-crack extension before cleavage varied from specimen to specimen. Figure 11 shows SEM photographs of the fracture surface of Specimen A-07, the specimen with the shortest ductile extension 0.1 mm (0.0039 in.). Figure 12 shows corresponding photographs for Specimen A-10, the specimen with the longest ductile extension 0.62 mm (0.024 in.). In some specimens, the solidification pattern of the weld metal appears to affect the fracture process, as illustrated in Figure 12c, which shows a region of elongated facets on the left of the fracture surface of Specimen A-10. The fracture appearance in this region suggests intergranular fracture along the boundaries of columnar grains.

Figure 13 shows the load versus crack-displacement curves measured in the tests at 0°C . The open circles along the curves represent AE events measured during each experiment. Fracture instability occurred at different stages of loading in each experiment. In Specimen A-07, instability occurred while the load was still rising (AE was not detected); in Specimen A-05, instability occurred at maximum load;

**Table 7. Fatigue-crack characteristics for
CRB tests at 0°C**

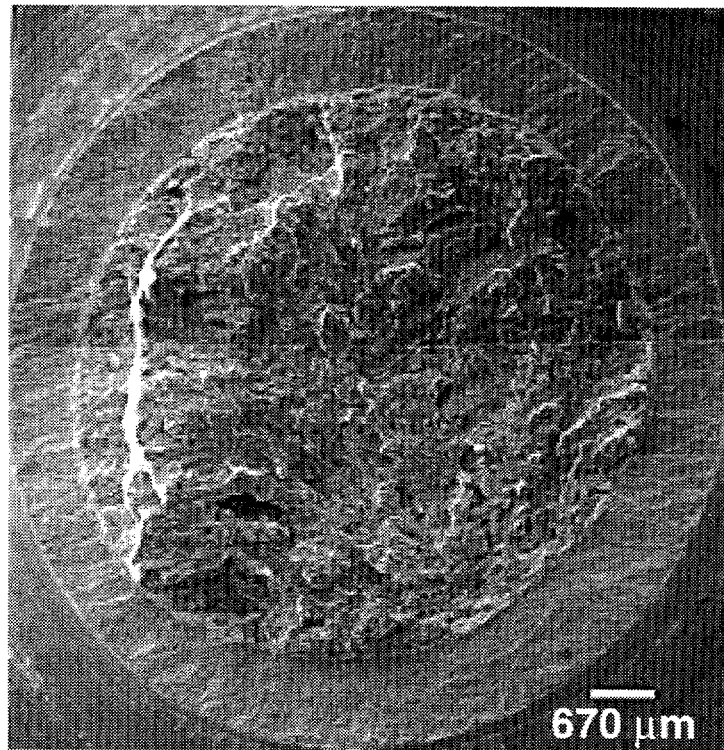
Specimen no.	Average crack depth (mm)	a/R	Eccentricity (mm)
A-03	5.46	0.69	0.36
A-05	5.14	0.65	0.13
A-07	4.79	0.60	0.10
A-10	4.72	0.59	0.25

in Specimens A-03 and A-10, instability occurred well beyond maximum load and was preceded by significant AE. We estimated the initiation toughness from the curves in Figure 13 using the first indication of AE to define the point of fracture initiation, except for Specimen A-05, for which we did not record any AE signal. In this case, we assumed that fracture initiation took place at maximum load, an assumption supported by the AE data in the other experiments. Table 8 lists the initiation toughness values we obtained. The experiments yielded consistent K values ranging from 173 to 182 MPa√m.

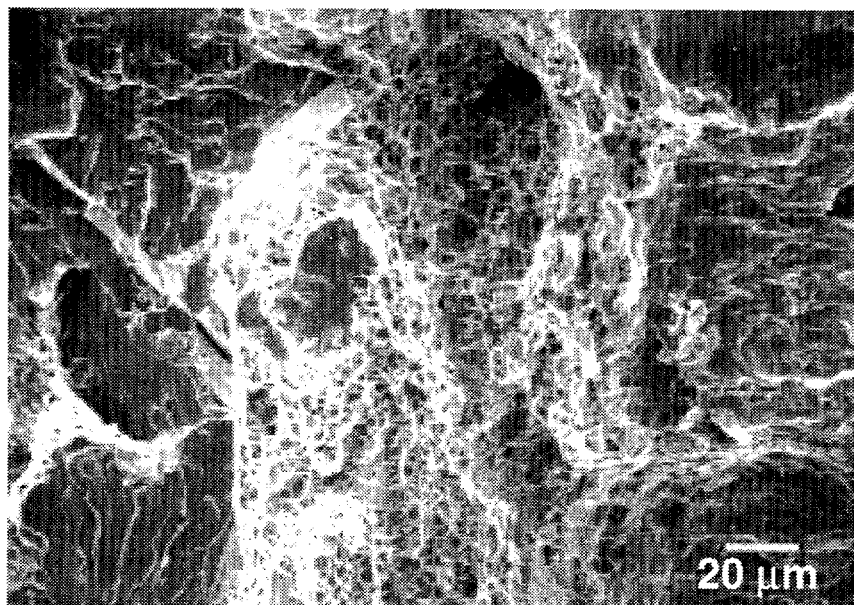
We also estimated a J resistance curve for ductile crack-growth from the experimental data for the tests at 0°C, applying the following procedure. First, we assumed that instability in the experiments corresponded to the onset of cleavage fracture. We then measured the length of the ductile crack at the ductile-cleavage fracture interface on the fracture surface, and we calculated with Equations (1) to (4) the J value corresponding to this crack length and the point of instability on the load versus crack-displacement curve. Columns 7 and 8 of Table 8 list the pairs of ductile crack growth and J values we obtained. Figure 14 shows the corresponding J-resistance curve (a linear fit to the experimental data points), together with the blunting line, which we constructed assuming a value of the flow stress equal to the average of yield and ultimate strength at 0°C; that is, 568 MPa (see Appendix A). The curve has a tearing modulus of 462. The value of J at initiation of 136 kJm⁻², given by the intersection of the blunting line and the resistance curve, is consistent with the values obtained directly in the experiments (column 3 of Table 8).

3.5 Test at 23°C

We performed only a single test at 23°C, with a specimen that had a deep crack and a significant eccentricity, as indicated in Table 9. In this specimen, fracture was initiated by ductile tearing and was switched to cleavage after 0.34 mm (0.0134 in.) of ductile crack growth.

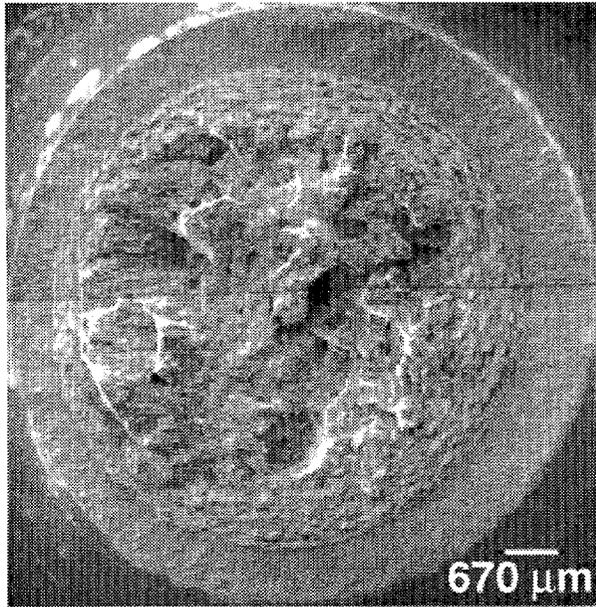


(a) Overall view of fracture surface.

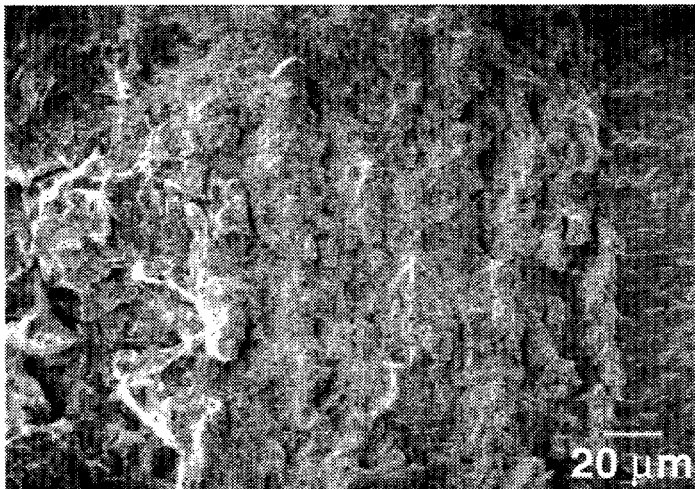


(b) Region near original fatigue crack tip showing narrow band of ductile voids.

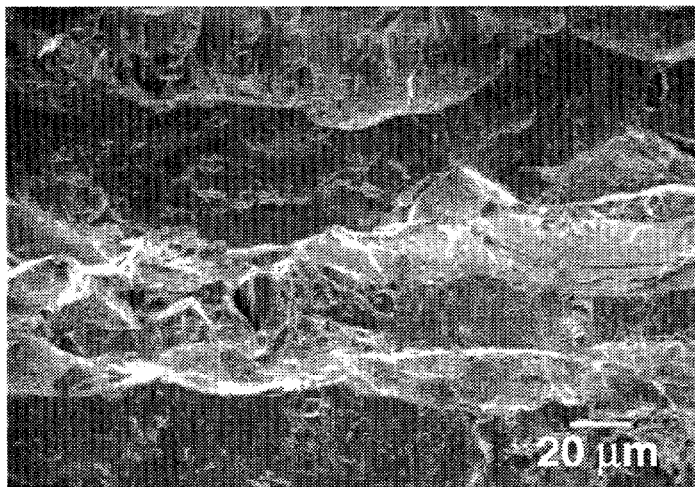
Figure 11. SEM photographs of Specimen A-07 tested at 0°C with the shortest ductile crack extension.



(a) Overall view of fracture surface.



(b) Region near original fatigue crack tip showing narrow band of ductile voids.



(c) Region with appearance of intergranular fracture along boundaries of columnar grains.

Figure 12. SEM photographs of Specimen A-10 tested at 0°C with the longest ductile crack extension.

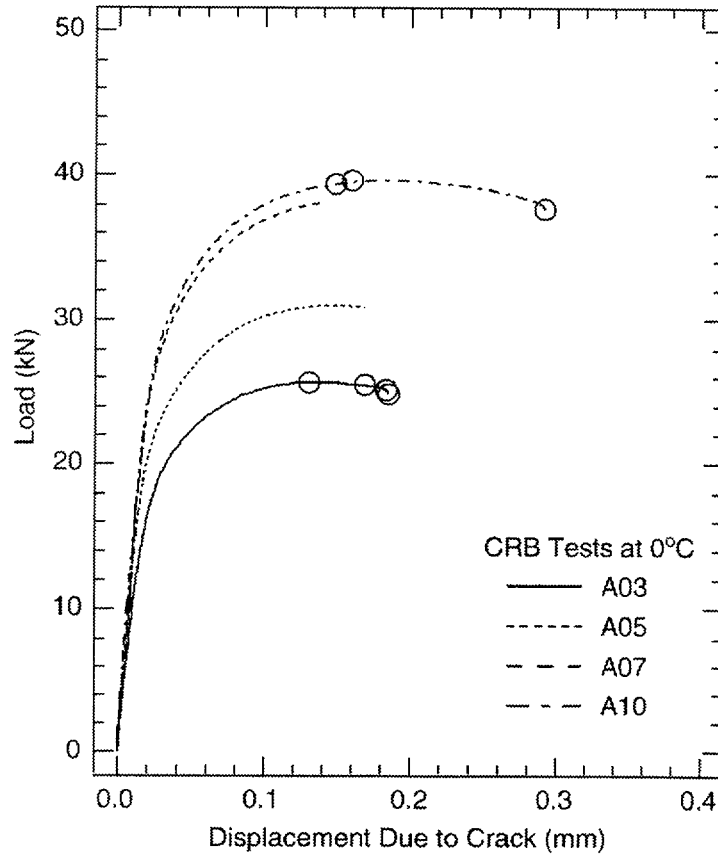


Figure 13. Load versus crack displacement for fracture experiments at 0°C.

Table 8. Results of CRB fracture experiments at 0°C

1	2	3	4	5	6	7	8
Specimen no.	Average radius of uncracked ligament (mm)	J at crack initiation, from AE signal (kJ/m ²)	J at peak load (kJ/m ²)	K from J of column 3 (MPa√m)	Average radius of cleavage zone (mm)	Average total depth of ductile crack growth (mm)	J at cleavage instability (kJ/m ²) ^a
A-03	2.48	130	130	173	2.14	0.34	265
A-05	2.79	143	143	182	2.58	0.21	200
A-07	3.14	128	128	172	3.04	0.10	137
A-10	3.16	141	189	180	2.54	0.62	504

^a Evaluated using the radius of the cleavage zone in column 6 at the point of instability.

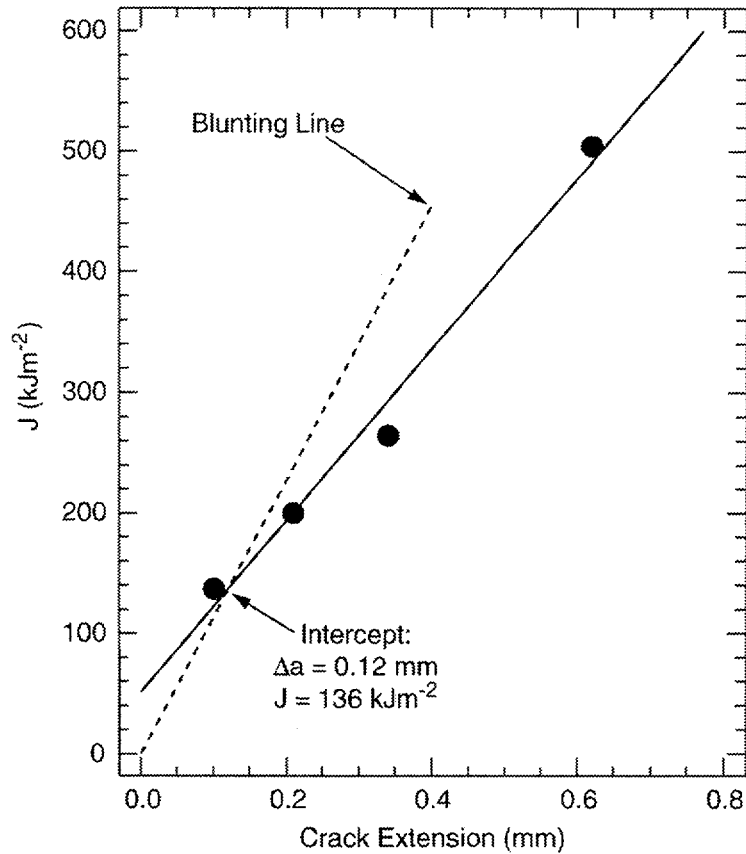


Figure 14. Pseudo J-resistance curve estimated from test data at 0°C.

Table 9. Fatigue-crack characteristics for CRB tests at 23°C

Specimen no.	Average crack depth (mm)	a/R	Eccentricity (mm)
A-06	5.29	0.67	0.37

Figure 15 shows the load versus crack-displacement curve for the 23°C experiment, as well as the corresponding J crack-displacement curve. Fracture instability occurred well beyond maximum load. For this test, we assumed that fracture initiation took place at maximum load and calculated an initiation toughness of $178 \text{ MPa}\sqrt{\text{m}}$. This value is probably a lower bound because of the significant amount of bending experienced by this specimen during the experiment (see the following discussion section and Appendix B). Table 10 lists the fracture data obtained.

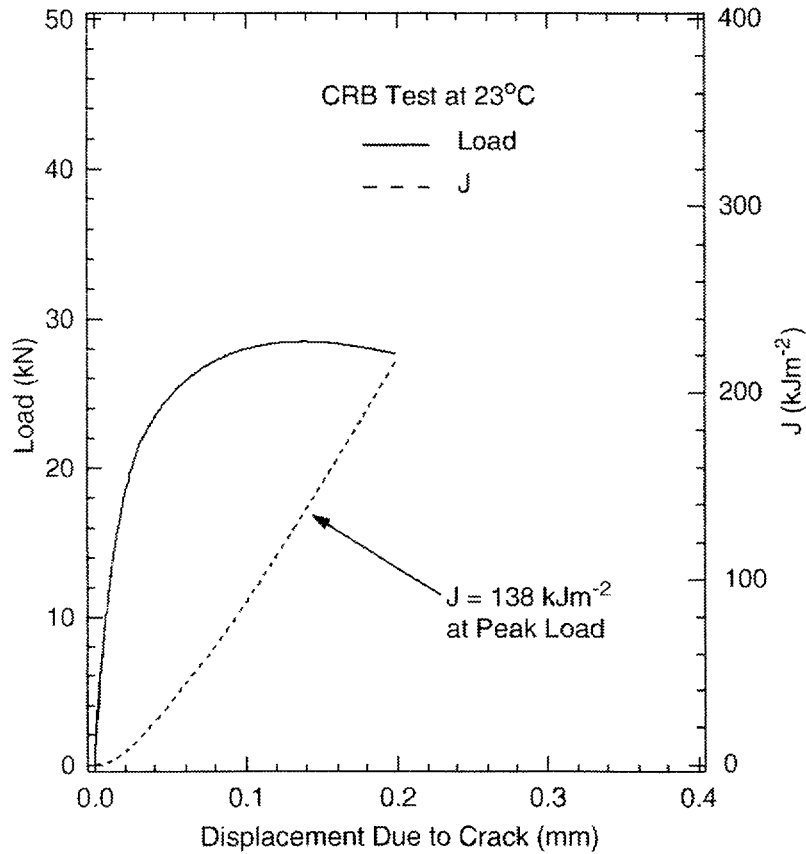


Figure 15. Load and J versus crack displacement for the fracture experiments at 23°C.

Table 10. Results of CRB fracture experiments at 23°C

1	2	3	4	5	6	7
Specimen no.	Average radius of uncracked ligament (mm)	J at peak load (kJ/m ²)	K from J of column 3 (MPa√m)	Average radius of cleavage zone (mm)	J at instability (kJ/m ²) ^a	Average depth of ductile crack growth (mm)
A-06	2.65	138	178	2.31	286	0.34

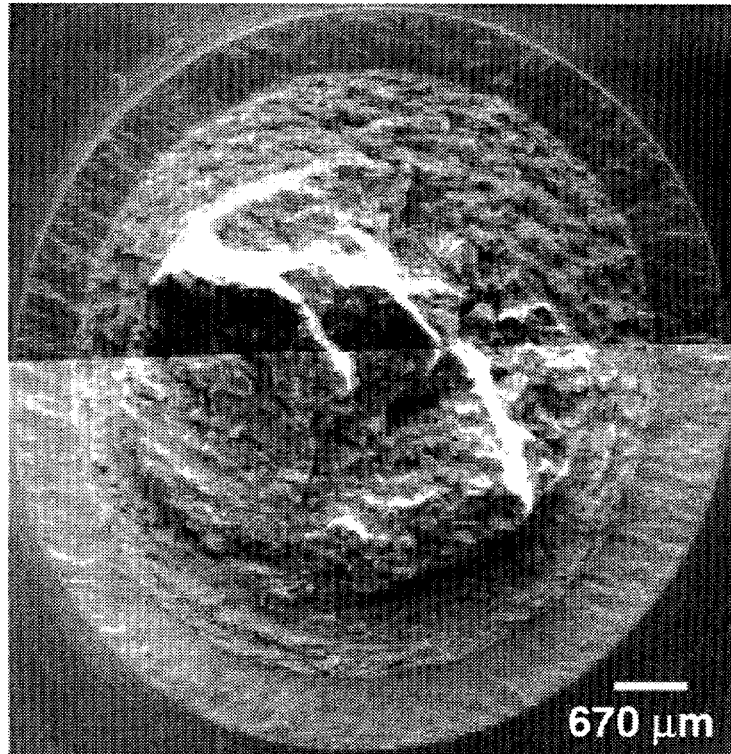
^aEvaluated using the radius of the cleavage zone in column 5 at the point of instability along the load-displacement curve.

3.6 Tests at 50°C

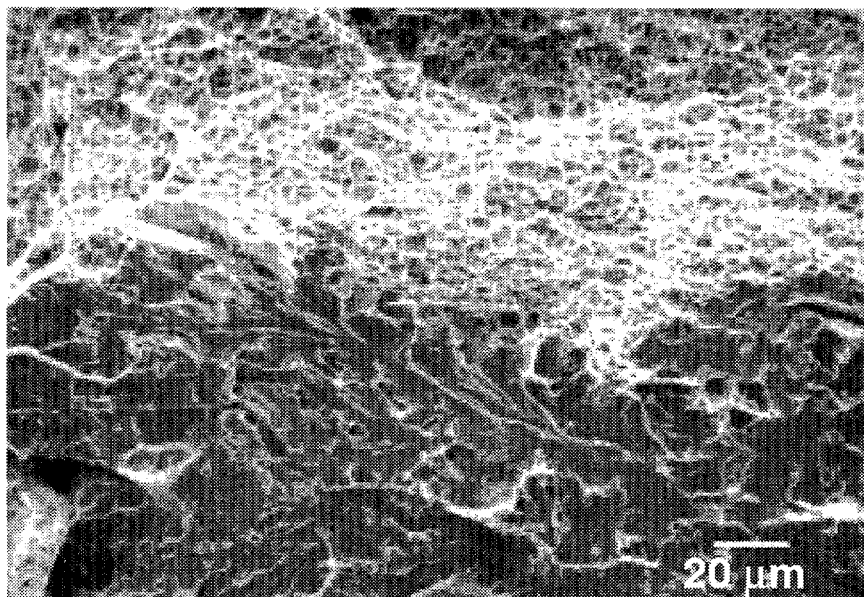
We tested six specimens at 50°C. Table 11 summarizes the characteristics of the fatigue cracks for these specimens. In these 50°C experiments, we did not record any meaningful AE that could be used to establish the point of fracture initiation. Therefore, we interrupted three of the tests before crack instability (C-01, C-02, and C-05) and performed partial unloadings during two experiments (B-08 and B-09) to establish when fracture initiates. Figure 16 shows a SEM photograph of the fracture surface of specimen B-07, a specimen for which unstable fracture took place well beyond maximum load. The fracture surface consists of an annular region of ductile tearing and central ligament that failed in cleavage. Additional fractographic observations on Specimen C-05 provided indications regarding the occurrence of ductile tearing during the unstable phase of fracture. For this specimen, we interrupted the test at peak load, heat-tinted the specimen, and then reloaded it dynamically (open-loop control on the servohydraulic testing system) to simulate the unstable phase of fracture. The fracture surface showed a region of ductile tearing several hundreds of micrometers long. However, the heat-tinted region of the fracture surface extended only about 100 μm from the crack tip, an amount that we can associate with blunting just before initiation. Therefore, the rest of the ductile tearing occurred during dynamic reloading of the specimen. From these observations we concluded that at 50°C (1) fracture does initiate at maximum load and (2) ductile tearing can occur during the unstable phase of fracture before the transition to cleavage fracture.

Table 11. Fatigue-crack characteristics for CRB tests at 50°C

Specimen no.	Average crack depth (mm)	a/R	Eccentricity (mm)
C-01	5.10	0.64	0.35
C-02	4.66	0.59	0.10
C-05	4.67	0.59	0.04
B-07	4.75	0.60	0.09
B-08	4.83	0.61	0.12
B-09	4.75	0.60	0.17



(a) Overall view of fracture surface.



(b) Ductile voids/cleavage transition region.

Figure 16. SEM photographs of Specimen B-07 tested at 50°C.

Figure 17 shows the load versus crack-displacement curves measured in the tests at 50°C. For clarity, the curves for Specimens B-08 and B-09 do not show the partial unloadings performed during the experiments. The serrations on the curve for Specimen C-05 represent creep unloadings that took place when we interrupted the test and held the machine-ram displacement constant. This low-temperature creep makes the control of the experiment quite difficult as the load approaches its maximum, particularly when the compliance of the loading system is large, as was the case in the current experiments.

As we mentioned earlier, unloading compliance records did not provide any reliable estimates of the current crack length during the experiment. On the other hand, we did establish that fracture initiation takes place at or near maximum load in the experiments at 50°C. Therefore, we calculated the initiation toughness on the basis of the J value at maximum load obtained from the load versus crack-displacement curves of Figure 17. Table 12 summarizes the results for the four specimens (B-07, B-08, B-09, and C-05) in which a crack was initiated during the experiment. Toughness values are consistent and range from 193 to 204 MPa√m.

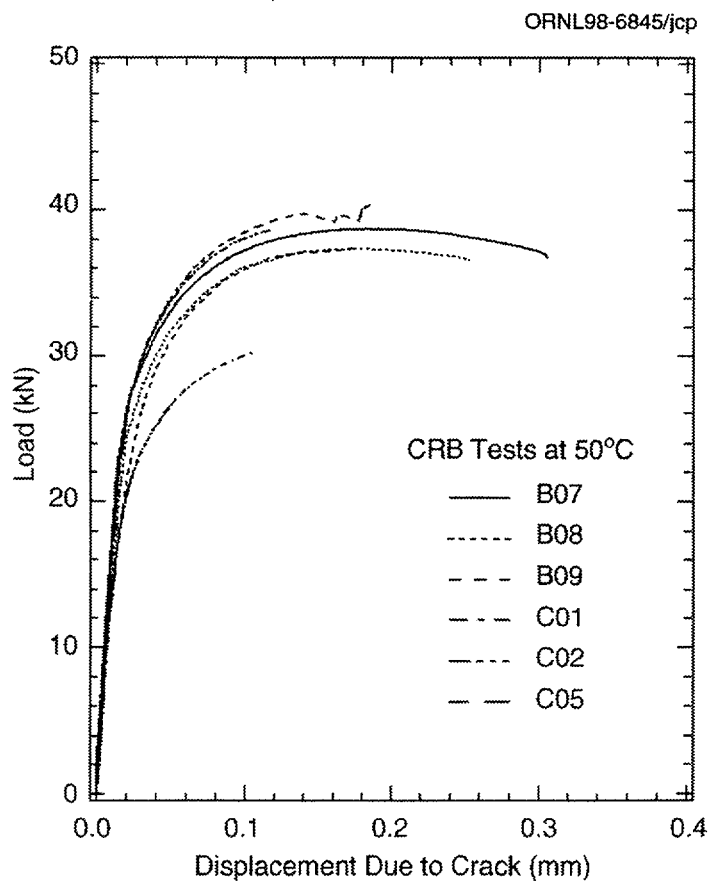


Figure 17. Load versus crack displacement for fracture experiments at 50°C.

Table 12. Results of CRB fracture experiments at 50°C

1	2	3	4	5	6	7
Specimen no.	Average radius of uncracked ligament (mm)	J at peak load (kJ/m ²)	K from J of column 3 (MPa√m)	Amount of crack growth at peak load ^a (μm)	Crack mouth opening displ. CMOD ^b (μm)	Comments
C-01	2.84	92	145	0	100	Interrupted test
C-02	3.28	99	151	0-50 blunting	100-120	Interrupted test
C-05	3.27	177	202	90-120 initiation	145-195	Interrupted test bending
B-07	3.19	182	204	NA	–	Unstable fracture after peak load
B-08	3.11	174	200	NA	–	2 partial unloadings, unstable fracture after peak load
B-09	3.19	162	193	NA	–	3 partial unloadings, unstable fracture at peak load, bending
^a Crack growth measured by hint-tinting the specimen after the test. ^b CMOD measured optically, after unloading of specimen, at four orthogonal locations around the circumference.						

For the experiments in which the test was interrupted before unstable fracture, we measured the crack mouth opening displacement (CMOD) of the unloaded specimens using an optical microscope. We compared these measurements with the extensometer values of the crack displacement corrected to account for elastic unloading. Table 12 lists the available CMOD values of the specimens. A range of values indicates that the CMOD was larger on one side than on the other and hence that the specimen underwent some bending. The optical and extensometer values on corresponding sides of the specimen agreed well. This agreement verifies the assumptions made in the experimental data-reduction procedure (estimation of δ_{cr}). The optical and extensometer measurements also both showed the same effect of specimen bending.

3.7 J-CMOD and J-CTOD Relationships

Finite-element analysis of the CRB specimen showed that the crack faces remain essentially straight and, in the absence of bending, parallel during loading. Therefore, we can assume that, at least in first

approximation, the CMOD is equal to the crack tip opening displacement (CTOD). Moreover, the analysis of the results of the experiments at 50°C and detailed fractographic results showed that δ_{cr} is a good measure of the CMOD and the CTOD. Therefore, the well-known proportionality relationship between J and CTOD should also apply to J and δ_{cr} , that is

$$J = \lambda \delta_{cr} \sigma_0 \quad , \quad (5)$$

where λ is a constant and σ_0 is the flow strength taken as the average of the yield and ultimate strengths at the given test temperature.

To verify this relationship experimentally, we generated J/σ_0 versus crack-displacement curves (where the crack displacement is the displacement derived from the extensometer measurements) for selected experiments at -80°, 0°, 23°, and 50°C, using the value of σ_0 for the appropriate test temperature taken from Reference 16. These curves are plotted in Figure 18 and represent lower-bound and upper-bound curves, except for the test at 23°C where only one curve was available. All the curves have the same shape (i.e., a parabolic curve in the elastic regime that gradually turns into a linear curve as we approach

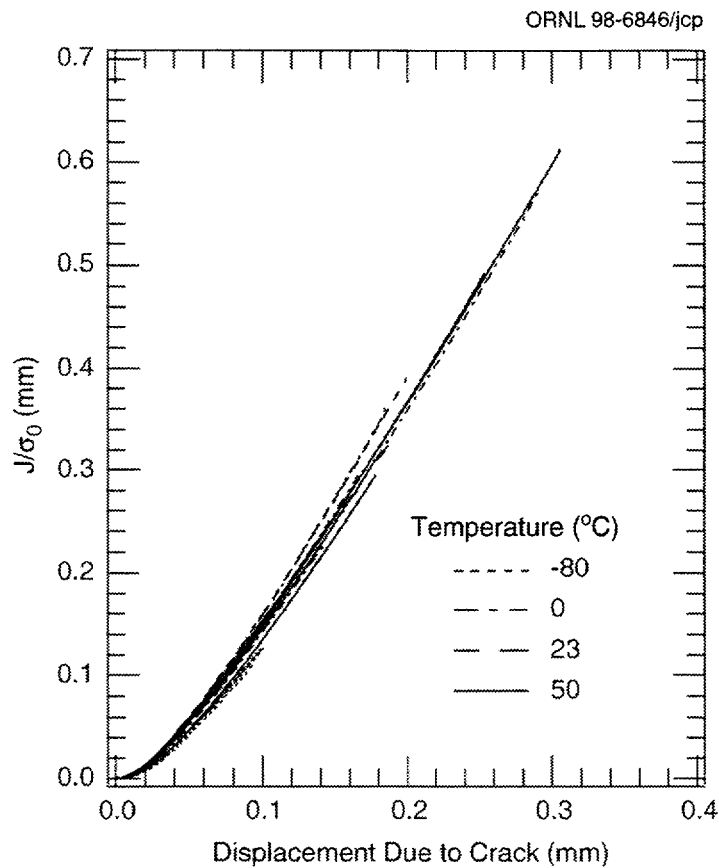


Figure 18. J/σ_0 versus displacement for selected specimens tested at -80°, 0°, 23°, and 50°C.

the fully plastic regime) and almost normalize to a single curve. The behavior of the J crack-displacement curves is not surprising. Indeed, theoretical considerations show that J varies as the square of the applied displacement (or CMOD) in the elastic regime and linearly in the fully plastic regime (see for example Reference 13).

We estimated the value of the constant λ by performing a least squares fit to the J (average) crack-displacement curves* of Figure 18. Table 13 summarizes the results of the estimation. We see that for the temperature range 0 to 50°C, the value of λ is reasonably constant and equal to 2.12 ± 0.13 , independent of temperature and crack depth. This value of λ is consistent with the proportionality factor in the plane strain J-CTOD relationship and is further evidence that δ_{cr} provides a good estimate of CTOD. λ values for tests at -80°C are much lower, which is not surprising because, at that temperature, the behavior is predominantly elastic and the J-displacement relationship is parabolic for elastic conditions. Therefore, fitting Equation (5) to the low temperature data is not really meaningful.

Table 13. Proportionality constant λ between J and δ_{cr}

Test temperature (°C)	σ_0 (MPa)	Specimen no.	λ
		B-02	1.649
-80	650	B-05	1.688
		C-03	1.689
		C-06	1.690
		A-03	2.280
0	568	A-05	2.119
		A-07	1.985
		A-10	2.197
23	556	A-06	2.281
		B-07	2.204
		B-08	2.206
50	546	B-09	2.024
		C-01	1.989
		C-02	1.922
		C-05	2.068

* Here we fitted only the part of the curve corresponding to values of J greater than 50 kJm⁻².

4. Discussion

In this discussion section, we first compare the CRB fracture-toughness data generated in this project with ORNL data obtained from tests with 1T-CT specimens, and in light of this comparison, we assess the potential of the CRB test for measuring valid plane strain fracture-toughness values. We then discuss additional significant findings and the experimental lessons learned during the feasibility study.

4.1 Comparison of ORNL 1T-CT Data and SRI CRB Data

Table 14 lists the 1T-CT toughness data provided by ORNL.¹⁶ Figure 19 compares the 1T-CT data obtained from ORNL with the CRB data generated by SRI. All the SRI data are toughness values derived from the J analysis of the fracture experiments, except for the data at -150°C , which represents data derived from a linear-elastic analysis. As mentioned in the Experimental Results Section, the CRB represent (to the best of our knowledge) true initiation fracture-toughness data (i.e., toughness at the onset of either ductile tearing or cleavage from an initially sharp fatigue crack). In contrast, the 1T-CT data represent toughness values at cleavage instability. Therefore, for the higher-test temperatures, the data may correspond to a significant amount of ductile tearing before cleavage.

In this discussion, we divide the CRB data into two groups: (1) data from the experiments at 0° , 23° , and 50°C , where fracture initiation occurs by ductile tearing and under conditions of extensive plasticity, and (2) data from experiments at -50° , -80° , and -150°C , where fracture initiation occurs by cleavage under conditions of limited plasticity.

Figure 19 indicates that, in the range 0° to 50°C , the CRB experiments yield ductile initiation toughness values that are lower and show less scatter than the limited data available from ORNL. This behavior may be explained by the fact that the ORNL data correspond to cleavage instability, occurring after some ductile-crack extension (i.e., at J values on the R-curve higher than the initiation value), whereas the SRI data strictly represent J or K values at ductile initiation. For completeness, we have also plotted, in Figure 19, the K values obtained in the CRB tests at cleavage instability. The ductile-initiation toughness values measured with CRB compare favorably with available data for pressure vessel steel in the corresponding temperature range. We can regard this consistency as evidence of the high degree of constraint that the CRB can develop in the fully plastic regime (see Reference 7).

For the group of experiments at -50° , -80° , and -150°C , CRB data are higher than the ORNL 1T-CT data, with the largest differences occurring at -80°C , and with closer agreement at -50° and -150°C . Also, the CRB toughness values at -80°C are somewhat higher than those at -50°C . We have not yet identified the exact reasons for these differences, but we suggest the following three sources.

**Table 14. Fracture-toughness data for HSSI Weld 72w (0.23% copper)
unirradiated obtained with 1T-CT specimens¹⁶**

Specimen no.	Test temperature (°C)	(a/W) ^a	Ductile crack extension (mm)	J @ cleavage (kJm ²)	K _{Jc} @ cleavage (MPa√m)
72W135	-150	0.522		6.9	38.6
72W138		0.522		7.0	39.0
72W113	-150	0.529		8.0	41.6
72W103	-101	0.525		10.3	46.8
72W168	-80	0.544		11.6	49.6
72W140		0.522		18.5	62.7
72W164		0.548		21.0	66.7
72W121		0.528		40.5	92.6
72W127		0.532		52.0	105.0
72W142	-80	0.512		53.0	106.0
72W105	-59	0.528	0.06	69.1	120.7
72W147	-50	0.538		44.0	96.1
72W156		0.540	0.06	64.9	116.8
72W154		0.526	0.07	67.1	118.7
72W157		0.530	0.06	68.2	119.7
72W148		0.516		70.6	121.8
72W153	-50	0.592	0.07	74.9	125.4
72W162	-30	0.537		50.4	102.6
72W158		0.528	0.08	76.2	127.8
72W131		0.530	0.11	93.5	139.7
72W133	-30	0.536	0.25	176.8	192.2
72W109	-26	0.526	0.11	96.9	142.2
72W161	-15	0.530		32.4	82.1
72W169		0.535		35.8	86.3
72W170		0.534	0.14	109.9	151.2
72W166	-15	0.525	0.15	136.8	168.7
72W165	0	0.511	0.11	79.9	128.7
72W151		0.525	0.13	124.0	160.3
72W128		0.529	0.34	209.8	208.5
72W160		0.512	0.71	300.0	249.0
72W159	0	0.520	0.66	329.0	261.0
72W111	23	0.520	0.92	387.6	282.5

^aa/W is the ratio of crack length to specimen width.

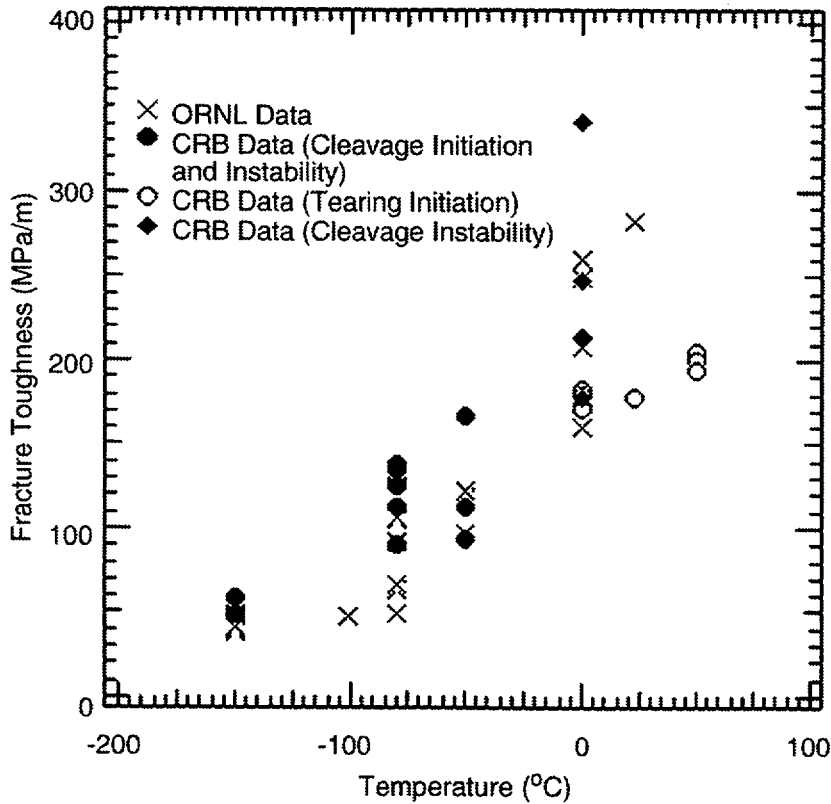


Figure 19. Comparison of ORNL 1T-CT and SRI CRB fracture data.

First, the analysis of the experiments at -150°C indicates a substantial discrepancy between toughness values obtained from the estimation of J using Equation (1) and those calculated with a linear-elastic fracture analysis. This discrepancy suggests that Equation (1) may not be accurate in the regime of contained plasticity characterizing the experiments at -80° and -50°C and thus may explain the observed overestimate of the toughness compared with the 1T-CT data.

Second, finite-element analyses of the CRB geometry show that during the early stages of plastic deformation, constraint in the CRBs is lower than in the three-point bend geometry. High constraint develops later when the CRBs become fully plastic. The difference in toughness values could therefore be caused by a difference in constraint between the CRBs and the CT specimen geometries for contained plasticity. However, earlier studies¹⁻⁴ have shown that CRBs give reliable toughness estimates under linear-elastic conditions. Therefore, there might only be an intermediate plasticity regime in which CRBs may not provide toughness values comparable with those measured with bend specimens.

Finally, cleavage-fracture initiation is a statistical process dependent on the presence of weak initiation sites ahead of the crack tip. As such, cleavage-fracture initiation demonstrates a so-called statistical-size effect (see, for instance, Reference 14), with smaller specimens yielding higher mean toughness values and having more data scatter. The CRBs have a shorter fatigue crack front length than the 1T-CT specimens so that we may expect somewhat higher toughness values.

The preceding three interpretations do not seem to account for the somewhat higher toughness values measured at -80°C compared with values at -50°C . However, additional tests at -50°C may well show broader scatter towards high toughness values than indicated by the present results and reconcile the data sets at -80° and -50°C . Note that the differences in toughness values at a given (low) temperature appear to correlate with the width of the narrow band of ductile voids near the original fatigue crack tip.

Clearly, additional analyses and experiments will be required to explain the present results. Nevertheless, the overall comparison between the IT-CT and the CRB data suggests that meaningful initiation-fracture toughness may be obtained with small CRBs for conditions on the lower shelf, as well as on the upper shelf.

4.2 Significance of J - δ_{cr} Proportionality

The present set of experiments shows that for the material tested and the range of temperatures 0 to 50°C where the specimens undergo large plastic deformations, there is a unique linear relationship between J and δ_{cr} . This result is significant in that it may allow a direct evaluation of the toughness from the experimental displacement measurements, thus simplifying the data reduction procedure. It also provides an approximate way to account for the effect of bending of the specimen when two displacement measurements are available, as is the case in the present experiments (see Appendix B).

4.3 Improvement in Experimental Method

Our study indicates that the analysis method based on Equation (1) must be thoroughly validated to determine its limitations, particularly in the small-scale yielding regime. We have acquired considerable experimental experience that can now be used to improve the test method. In particular, our method of monitoring the tensile compliance of the specimen at regular intervals during precracking affords an accurate control of the crack depth. In this way, we can reliably introduce fatigue cracks with the desired optimum depth of about 1 mm (0.039 in.). This improved control of the fatigue crack depth also results in reduced eccentricities because deep cracks with small remaining ligaments are more eccentric than shallower cracks.

We also learned that the loading conditions for the specimen are quite sensitive to the gripping arrangement. Small misalignment in the threaded grips and the load train can introduce significant bending of the specimen, even with a well-centered remaining ligament. The approximate analysis presented in Appendix B suggests that for most of the test conditions of this study, neglecting the effect of bending introduces errors of no more than 10% on the toughness values. Moreover, the values estimated with neglecting the bending effects represent lower bounds. Nevertheless, we must improve the gripping method in order to remove this undesired loading feature.

The configuration of the loading train influences the onset of fracture instability and the creep processes in the specimen during displacement hold periods near maximum load. As a result, the configuration of the loading train may affect the ability to detect crack initiation and small amounts of crack growth.

Our experimental results provide strong evidence that for the specimen geometry and size used, and in the range of temperatures and deformation levels considered, fracture initiation occurs at or very near maximum load. This assertion is further supported by the analysis presented in Appendix C. The smaller the specimen, the likelier it is that fracture initiation coincides with maximum load. Initiation at maximum load again offers the possibility for simplified testing methods by eliminating the need to monitor crack length to obtain initiation toughness values. This represents an appreciable advantage because our results suggest that it may be difficult to perform reliable crack growth measurements in small CRB specimens. Indeed, the unloading compliance method gave inconsistent data, and we experienced some difficulty in interrupting tests at different levels of deformation to evaluate the crack extension because of the pronounced creep and the speed of deformation at and past maximum load.

The results of our feasibility study indicate that small CRBs may be suitable for reliably measuring initiation toughness values over a wide range of temperatures and deformation levels. However, size limitation for the CRB geometry should be investigated. The minimum size of CRB specimens may be limited by several considerations, such as constraint and stress state effects, ratio of characteristic microstructural dimensions to uncracked ligament, and crack front length and statistical effects (for cleavage initiation). Further consideration of size limitations for CRB specimens is, however, beyond the scope of this feasibility study but should be undertaken.

Finally, we should comment on the experience gained with AE measurements to detect fracture initiation. The test series at 0°C provided unambiguous AE signals traceable to the crack plane, which we associated with the onset of ductile tearing in the specimens. On the other hand, the test series at 50°C gave no meaningful AE results despite the fact that significant ductile tearing also occurred in these experiments.* Therefore, we speculate that temperature may affect the process of void coalescence. In other words, at lower temperatures, the final coalescence process is more abrupt and releases elastic energy more suddenly than at higher temperatures. This interpretation is consistent with the strength variation with temperature and with our observation of increased creeping rates during hold periods at higher temperature: lower strength and creep relaxation will make the coalescence process more gradual and reduce the elastic-strain energy released during the final coalescence phase.

* We made the same observation in tests performed in a separate program on a bridge steel weldment (Reference 15).

5. Conclusions and Recommendations

5.1 Conclusions

The initiation fracture-toughness values obtained for HSSI Weld 72W, unirradiated, in the temperature range of -150 to 50°C , with small CRB specimens agree well with the values obtained with 1T-CT specimens. This agreement indicates that measuring reliable fracture-toughness values with small specimens cut from Charpy bars may be feasible. Therefore, the use of the CRB test may allow us, for the first time, to (1) obtain direct toughness values from small irradiation-surveillance specimens and (2) perform more accurate fracture analysis of older nuclear pressure vessels.

5.2 Recommendations

In view of the encouraging results of this feasibility study, we recommend that the development of the CRB test method be continued. This effort should start with an analytical task to (1) validate the J evaluation formulas, (2) guide the design of small specimens that can be fabricated from broken Charpy specimens, (3) generate compliance functions, (4) evaluate constraint as a function of material properties (strength and hardening) and deformation level, and (5) establish size requirements.

The effort should then focus on developing and validating a test method for small specimens fabricated from broken halves of Charpy bars. Experimental issues to resolve include the following:

- Design of extension bars to grip the short specimen during fatigue precracking
- Selection of optimum specimen geometry and dimensions
- Development of a reliable precracking procedure
- Development of an improved gripping method to suppress bending during fracture testing
- Development of methods to monitor crack extension (for example DC potential drop)
- Experimental validation of the test procedure by comparing CRB toughness data with data obtained for the same material with 2T or larger CT specimens.

As a further step, we recommend that the development of dynamic testing methods for CRBs also be considered because the specimen geometry is ideally suited for high rate testing.

Dynamic fracture-toughness values will provide lower bounds to include in the ASME Pressure Vessel Code. They will also permit a more realistic assessment of the likelihood for reinitiation of an arrested crack under pressurized thermal shock conditions.

6. References

1. H. L. Stark and R. N. Ibrahim, "Estimating Fracture Toughness from Small Specimens," *Engineering Fracture Mechanics* **25**, 395–401 (1986).
2. R. N. Ibrahim and H. L. Stark, "Validity Requirements for Fracture Toughness Measurements Obtained from Small Circumferentially Notched Cylindrical Specimens," *Engineering Fracture Mechanics* **28**, 455–460 (1987).
3. R. N. Ibrahim and H. L. Stark, "Establishing K_{Ic} from Eccentrically Fatigue Cracked Small Circumferentially Grooved Cylindrical Specimens," *International Journal of Fracture* **44**, 179–188 (1990).
4. Y. C. Lam and R. N. Ibrahim, "Improvement of the Fracture Toughness of an Aluminum Alloy," *Fatigue Fract. Engng. Mater. Struct.* **17**, 277–284 (1994).
5. J. C. Devaux, G. Rousselier, F. Mudry, and A. Pineau, "An Experimental Program for the Validation of Local Ductile Fracture Criteria Using Axisymmetrically Cracked Bars and Compact Tension Specimens," *Engineering Fracture Mechanics* **21**, 273–283 (1985).
6. F. M. Beremin, "Calculation and Experiment on Axisymmetrically Cracked Tensile Bars: Prediction of Initiation, Stable Crack Growth and Instability," in Transactions of the 6th International Conference on Structural Mechanics in Reactor Technology, Vol. L, paper L 6/2 (1981).
7. J. H. Giovanola, H. Homma, M. Lichtenberger, J. E. Crocker, and R. W. Klopp, "Fracture Toughness Measurements Using Small Cracked Round Bars," *Constraint Effects in Fracture: Theory and Applications*, ASTM STP 1244, Mark Kirk and Ad Bakker Eds., American Society for Testing and Materials, Philadelphia, 1994.
8. L. S. Costin, J. Duffy, and L. B. Freund, "Fracture Initiation in Metals Under Stress Wave Loading Conditions," pp. 301–318 in *Fast Fracture and Crack Arrest*, ASTM STP 627, G. T. Hahn and M. F. Kanninen, Eds., American Society for Testing and Materials, Philadelphia, 1977.
9. R. H. Hawley, J. Duffy, and C. F. Shih, "Dynamic Notched Round Bar Testing," pp. 275–282 in *ASM Metals Handbook*, 9th ed., Vol. 8, Mechanical Testing, American Society for Metals, Metals Park, Ohio, 1985.
10. P. Bensussan, "Rupture Dynamique de L'acier 35 NCD16," in *Dymat 88, Second International Conference on Mechanical and Physical Behavior of Materials Under Dynamic Loading—Ajacio*, 1988; *Journal de Physique*, Colloque C3, 1988, supplément au *Journal de Physique III*, n° 8, les Éditions de Physique, Les Ulis Cedex A, France, pp. C3-199 to C3-206.

11. H. Tada, P. C. Paris, and G. R. Irwin, *The Stress Analysis of Cracks Handbook*, Del Research Corporation, St. Louis, 1973.
12. J. R. Rice, P. C. Paris, and J. C. Merkle, "Some Further Results of J Integral Analysis and Estimates," pp. 231–245 in *Progress in Flaw Growth and Fracture Toughness Testing, ASTM STP 536*, American Society for Testing and Materials, Philadelphia, 1973.
13. R. J. Bucci, P. C. Paris, J. D. Landes, and J. R. Rice, "J Integral Estimation Procedures," pp. 40–69 in *Fracture Toughness, Proceedings of the 1971 National Symposium on Fracture Mechanics, Part II, ASTM STP 514*, American Society for Testing and Materials, 1972.
14. J. D. Landes and D. H. Shaffer, "Statistical Characterization of Fracture in the Transition Region," pp. 368–382 in *Fracture Mechanics, Twelfth Conference, ASTM STP 700*, American Society for Testing and Materials, 1980.
15. T. Kobayashi, D. A. Shockey, J. H. Giovanola, and J. E. Crocker, "Relating Acoustic Emission Signals to Microfailure Events: Obtaining More Information on Bridge Integrity from Self-Monitoring Systems," Quarterly Report No. 5, Prepared for the Federal Highway Administration, Contract DTFH61-93-X-00037, SRI Project 4914, December 1994.
16. R. K. Nanstad, F. M. Haggag, D. E. McCabe, S. K. Iskander, K. O. Bowman, and B. H. Menke, Martin Marietta Energy Systems, Oak Ridge Natl. Lab., *Irradiation Effects on Fracture Toughness of Two High-Copper Submerged-Arc Welds, HSSI Series 5*, USNRC Report NUREG/CR-5913 (ORNL/TM-12516/VI), 1992.

Appendix A. Composition and Tensile Properties of HSSI Weld 72W (0.23% Copper) Unirradiated

The information provided in this appendix was abstracted from U.S. Nuclear Regulatory Commission Report NUREG/CR-5913.* The weld was fabricated for Oak Ridge National Laboratory's Heavy-Section Steel Irradiation (HSSI) Series 5 program.

The weld was fabricated with a weld wire specially produced by Combustion Engineering, Inc., CE-Wire, Norcross, Georgia. The wires were 4 mm (0.156 in.) in diameter and conformed to American Welding Society Specification A5.23-80, Electrode Classification EF-2, with additional chemical composition requirements: (1) Ni = 0.6 to 0.7 wt %, (2) Cu = 0.20 to 0.25 wt %, (3) P = 0.012 wt % max, and V = 0.05 wt % max. The wire heat number is 87984. The weld was fabricated in A533 grade B class 2 plate (Lukens Steel Co., Coatesville, Pennsylvania., Melt No. B2511) of 218-mm (8.6-in.) thickness by Combustion Engineering, Inc., Chattanooga, Tennessee, using the submerged-arc process with one lot of Linde 0124 flux (20 × 150 mesh, lot No. 01033) supplied by Combustion Engineering. The weld was fabricated with a tandem-arc, alternating current procedure using a 0-degree bevel weld groove with a heat input of 4 MJ/m (101.5 kJ/in.) and a travel speed of 0.56 m/min (22 in./min). All welds were postweld heat-treated at 607°C (1125°F). The complete chemical composition of the base metal and weld is given in Table A-1. The weld microstructure is generally bainitic with some ferrite islands. Table A-2 and Figure A-1 present the tensile properties of the weld.

* R. K. Nanstad, F. M. Haggag, D. E. McCabe, S. K. Iskander, K. O. Bowman, and B. H. Menke. "Irradiation Effects on Fracture Toughness of Two High-Copper Submerged-Arc Welds, HSSI Series 5," USNRC Report NUREG/CR-5913 (ORNL/TM-12516/VI), 1992.

Table A-1. Chemical compositions of submerged-arc Weld HSSI 72W (0.23% copper) unirradiated

Material	Composition ^{a,b} (wt %)													
	C	Mn	P	S	Si	Cr	Ni	Mo	Cu	V	Co	Al	An	Sn
72W mean	0.093	1.60	0.006	0.006	0.44	0.27	0.60	0.58	0.23	0.003	0.030	0.006	0.002	0.003
σ	0.006	0.038	0.0005	0.0005	0.024	0.008	0.008	0.008	0.006	0.0004				
Base metal ^c	0.021	1.24	0.008	0.004	0.23	0.12	0.66	0.56	0.11	0.003	0.015	0.040	0.007	0.008

^aFor all materials, the following additional elements were determined: Cb < 0.01, Ta < 0.01, Ti < 0.01, B < 0.001, W < 0.01, and Zr < 0.001.

^bMean and standard deviations (σ) shown result from 84 separate analyses for 72W taken from different locations through weldments.

^cSA-533 grade B class 2 Lukens Melt No. B2511.

Table A-2. Tensile properties of HSSI Weld 72W unirradiated

Test temperature (°C)	Specimen no.	Yield strength (MPa)	Ultimate strength (MPa)	Uniform strain (%)	Total elongation (%)	Reduction of area (%)
	72W278	739	816	13	28	61
-150	72W276	730	817	13	27	62
	72W280	731	825	13	27	61
	72W251	606	728	12	25	65
-101	72W253	598	739	13	25	66
	72W255	602	743	12	25	64
	72W257	552	689	12	21	63
-58	72W259	560	695	11	22	66
	72W260	577	713	11	23	65
	72W267	526	649	9	20	66
-26	72W263	524	649	10	22	64
	72W265	530	657	10	23	66
	72W274	495	602	8	21	69
28	72W269	499	606	8	20	68
	72W271	499	610	8	20	65

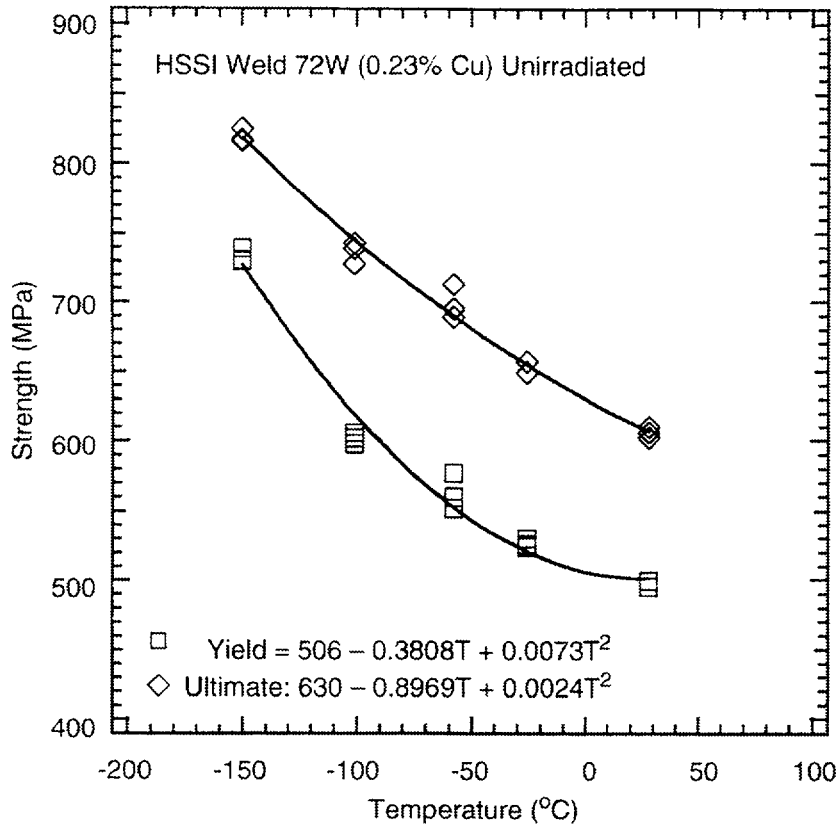


Figure A.1. Temperature dependence of the yield and ultimate strengths for HSSI Weld 72W (0.23% copper) unirradiated.

Appendix B. Analysis of the Effect of Bending on J Values in Cracked Round Bar Experiments

Neglecting bending effects introduced by loading fixture misalignment and crack eccentricity may lead to underestimated initiation toughness values. Here, we present a simple analysis to evaluate the effect of bending.

B.1 Bending Caused by an Eccentric Ligament: Fully Plastic Case

We evaluate the effect on initiation toughness values measured in cracked round bar (CRB) experiments of neglecting bending caused by an eccentric ligament. First, we consider tests conducted in the fully plastic regime. We assume that the tested material is rigid-perfectly plastic with a flow stress σ_{flow} . This assumption implies that all the plastic deformation is localized on the uncracked ligament. Further, we assume that the customary relationship between J and crack tip opening displacement (CTOD) given by Equation (5) holds. This assumption is supported by the data presented in the body of this report (Table 13).

We then express the CTOD in terms of the two (axial) displacements, δ_1 and δ_2 , measured at both ends of the specimen on a diameter normal to the neutral axis. With reference to Figure B-1, we consider a circular uncracked ligament of radius r_0 . The center of the ligament is displaced by ϵ with respect to the center of the original specimen cross section. The neutral axis of the ligament subjected to tension and bending is situated at a distance αr_0 from the center of the ligament.

We define the average displacement as

$$\delta_{\text{av}} = \frac{\delta_1 + \delta_2}{2} \quad (\text{B-1})$$

and the rotation as

$$\theta \approx \tan(\theta) = \frac{\delta_1 - \delta_2}{2 R_0} \quad (\text{B-2})$$

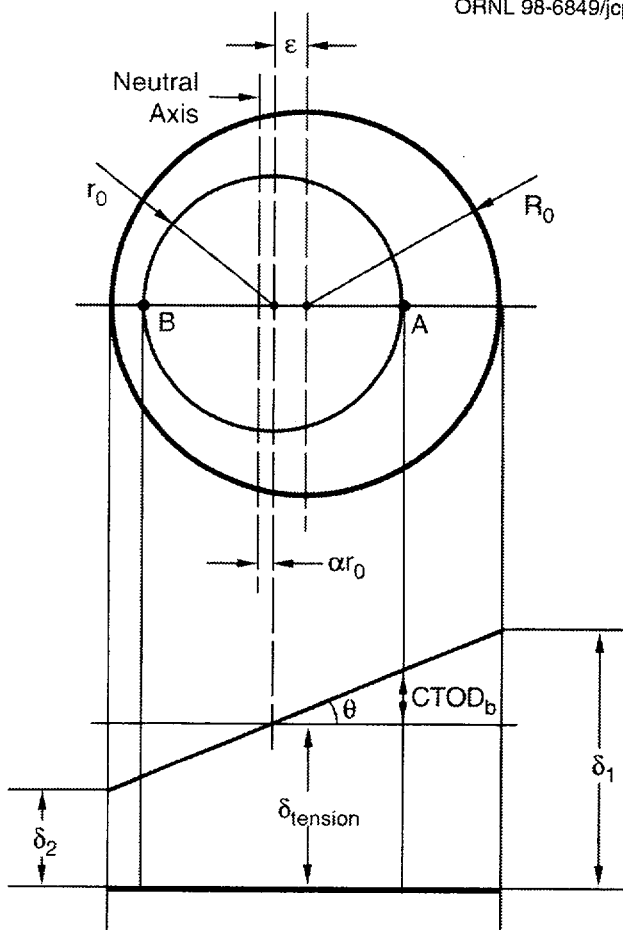


Figure B.1. Geometry of the rigid plastic deformation of the cracked round bar specimen with eccentric ligament.

The component of the displacement caused by pure tension is then

$$\delta_{\text{tension}} = \frac{(R_0 + \epsilon) \delta_2 + (R_0 - \epsilon) \delta_1}{2 R_0} , \quad (\text{B-3a})$$

$$= \delta_{\text{av}} - \epsilon \left(\frac{\delta_1 - \delta_2}{2 R_0} \right) , \quad (\text{B-3b})$$

and

$$= \delta_{\text{av}} - \tan(\theta) \epsilon \quad (\text{B-3c})$$

Assuming that the crack faces remain straight, as shown earlier, the tensile component of the CTOD at points A and B of the crack front in Figure B-1 is given by Equations (B-3a through B-3c), and the bending component is given by

$$(\text{CTOD})_b = r_0 \tan(\theta) = \frac{r_0}{2 R_0} (\delta_1 - \delta_2) . \quad (\text{B-4})$$

Combining Equations (5), (B-3), and (B-4), we obtain

$$\frac{J_b}{J_t} = \frac{(\text{CTOD})_b}{(\text{CTOD})_t} = \frac{r_0(\delta_1 - \delta_2)}{(R_0 + \epsilon)\delta_2 + (R_0 - \epsilon)\delta_1} = \xi . \quad (\text{B-5})$$

Thus

$$J = J_t + J_b = J_t (1 + \xi) , \quad (\text{B-6})$$

and the relative contribution of bending to the toughness is then

$$\frac{K_b}{K} = \frac{K - K_t}{K} = \frac{\sqrt{J} - \sqrt{J_t}}{\sqrt{J}} = 1 - \sqrt{\frac{1}{1 + \xi}} . \quad (\text{B-7})$$

We can use Equations (B-5) and (B-7) together with experimental values of e , d_1 , and d_2 to estimate the error on the toughness measured with CRB specimens with eccentric ligaments. Applying the analysis to the data in this report, we estimate that for typical eccentricities measured in CRBs the error made in neglecting the bending component of J is rather small (less than 5%) for specimens of pressure-vessel steel and weldment tested in the fully plastic regime. Results for Specimens A-10 and A-07 tested at 0°C are summarized in Table B-1.

Table B-1. Error estimate for two CRB tests at 0 °C

	Test A-10	Test A-07
R_0 (mm)	7.94	7.94
r_0 (mm)	3.22	3.15
ϵ (mm)	0.28	0.10
δ_1 (mm)	0.28	0.21
δ_2 (mm)	0.18	0.17
α	0.8336	0.9090
ξ	0.089	0.042
Equation (B-7) error	$\approx 4.2\%$	$\approx 2\%$

Further, in calculating J from the experimental data, we use the average displacement d_{av} given by Equation (B-1). This displacement is equal to the tensile component of the CTOD to which a corrective term is added in Equation (B-3). The corrective term can be regarded as an estimate of the bending component of the CTOD to which it is related by the equation

$$\frac{(\text{CTOD})_{b\text{-corr}}}{(\text{CTOD})_b} = \frac{\epsilon}{r_0} \quad (\text{B-8})$$

The data reduction procedure based on the use of the average displacement d_{av} accounts implicitly for some of the bending displacement. Therefore, the error on the toughness values should be slightly smaller than indicated previously for tests meeting the assumptions underlying the analysis.

B.2 Elastic Loading Case

In the case of elastic loading, an upper bound to the error introduced by neglecting the bending effect can be obtained from the Handbook solution for the CRB subjected to bending,* with the bending moment given by

$$M = P\varepsilon \quad .$$

This formulation assumes that the bending introduced by eccentricity is allowed to develop fully, that is, that the ends of the CRB specimen are allowed to rotate. Then the ratio of the stress intensity factors caused by bending and tension, respectively is

$$\frac{K_b}{K_t} = \frac{4\varepsilon}{r_0} \frac{G(r_0/R_0)}{F(r_0/R_0)} \quad , \quad (\text{B-9})$$

where the nondimensional functions G and F are given in the Handbook.* For Test C-10 at -150°C ($\varepsilon = 0.19$), we estimate an error K_b/K_t of about 15%. Because of loading train realignment and rigidity in the gripping arrangement, it is likely that the effective moment applied to the specimen is less than assumed here and hence that the error is smaller, on the order of 10%.

* H. Tada, P. C. Paris, and G. R. Irwin, *The Stress Analysis of Cracks Handbook*, Del Research Corporation, St. Louis, 1973.

Appendix C. Analysis of Conditions at Maximum Load in CRB Tests

In this appendix, we present a simple analysis of the cracked round bar (CRB) behavior near maximum load to provide evidence that little or no crack growth occurs before maximum load.

We can express the load on the CRB specimen as

$$P = \pi (R_0 - a)^2 \sigma_0 \quad , \quad (C-1)$$

where a is the crack depth and the other symbols have been defined previously in this report. Here σ_0 represents the average stress across the remaining ligament under the fully plastic conditions. Then the change in load is

$$dP = -2\pi (R_0 - a) \sigma_0 da + \pi (R_0 - a)^2 d\sigma_0 = 0 \quad , \quad (C-2)$$

and the second equality is valid at maximum load. Maximum load can be reached because (1) strain hardening has saturated, i.e., $d\sigma_0 \leq 0$, (2) the reduction in net section caused by crack extension decreases the load-carrying capability faster than the increase caused by hardening, and (3) both the net section and the flow stress decrease.

Let us assume that $d\sigma_0 > 0$ and that the flow stress is given by a power-law hardening constitutive equation; that is,

$$\sigma_0 = \sigma_y \left(\frac{\epsilon}{\eta \epsilon_y} \right)^{1/n} \quad (C-3)$$

Introducing Equation (C-3) into Equation (C-2) yields

$$\frac{dP}{\sigma_0} = -2\pi (R_0 - a) da + \pi (R_0 - a)^2 \frac{d\epsilon}{\epsilon n} \quad (C-4)$$

Therefore, the load P will rise or be a maximum if

$$da \leq \frac{R_0 - a}{2n} \frac{d\epsilon}{\epsilon} \quad (C-5)$$

Let us further assume that

$$\frac{d\varepsilon}{\varepsilon} \approx \frac{d\delta_{cr}}{\delta_{cr}}, \quad (C-6)$$

so that Equation (C-5) becomes

$$da \leq \frac{R_0 - a}{2n} \frac{d\delta_{cr}}{\delta_{cr}} \quad dP \geq 0 \quad (C-7)$$

In other words, the load will continue to rise after crack initiation if the crack-growth increment is smaller than the right hand side of Equation (C-7).

First, we note that the amount of crack extension that can occur before maximum load depends on the absolute size of the specimen (the radius of the remaining ligament $R_0 - a$). Therefore, the smaller the specimen, the less likely it is to experience stable crack extension before maximum load. Next, we apply Equation (C-7) to Test A-10, performed at 0°C, in which the specimen deformed well past maximum load. We estimate the increment of crack growth that may have occurred between initiation and maximum load, assuming initiation at a displacement $\delta_{cr-init} = 0.15$ mm (0.006 in.), whereas maximum load was reached at $\delta_{cr-max} \approx 0.23$ mm (0.009 in.) (see Figure 13). Taking the appropriate values of R_0 8 mm (0.315 in.), a 4.72 mm (0.186 in.), and $n = 10$ (a typical value for pressure-vessel steels), we estimate that the crack would have grown at most 70 to 80 μ m before reaching maximum load. This crack-growth increment is rather small and comparable to the width of the stretch zone caused by blunting of the initial fatigue crack. Therefore, the analysis indicates that determining initiation toughness values at maximum load is an acceptable procedure for the size of specimens used in this study.

Noting that

$$\frac{da}{d\delta_{cr}} \approx \frac{da}{dCTOD} \quad \text{and} \quad \delta_{cr} \approx CTOD \quad (C-8)$$

we can rewrite Equation (C-7) as

$$\frac{da}{dCTOD} \leq \frac{R_0 - a}{2n(CTOD)_{init}} \quad (C-9)$$

or, using Equation (5), as

$$da \leq dj \frac{R_0 - a}{2nJ_{lc}} \quad \text{for } dP \geq 0 \quad \text{or} \quad \Delta a \leq (J_{\max \text{ load}} - J_{lc}) \frac{R_0 - a}{2nJ_{lc}} \quad \text{for } \Delta P \geq 0 \quad . \quad (C-10)$$

Equation (C-10) gives a bound for the amount of crack growth before maximum load in terms of J values at initiation and maximum load. Using the data from tests at 50°C (Test C-02, $J_{lc} = 99 \text{ kJm}^{-2}$, Test B-07 $J_{\max \text{ load}} = 182 \text{ kJm}^{-2}$), we estimate a value of Δa of 134 μm , which is close to the value measured by heat-tinting in Specimen C-05. The experiment was interrupted at maximum load for this specimen.

The previous analyses are based on load equilibrium considerations. We can also perform a tearing stability analysis, following the procedure of Paris et al.* For the CRB of length L , the applied tearing modulus is

$$T_{\text{appl}} = \frac{2}{\Omega} \left(\frac{\sigma_{ct}}{\sigma_0} \right) (R_0 - a) \left(\frac{L}{R_0^2} + EC_m \right) \quad , \quad (C-11)$$

where σ_{ct} represents the elevated flow strength at the crack tip and w is a coefficient relating the CTOD to the specimen elastic displacement, δ_{el} ; that is, $\delta_{ct} = \omega \text{ CTOD}$, and C_m is the compliance of the loading system. For

$$\frac{(R_0 - a)}{R_0} < \frac{1}{\sqrt{3}} \quad , \quad \text{we have} \quad \frac{1}{\Omega} \left(\frac{\sigma_{ct}}{\sigma_0} \right) > 6$$

so that

$$T_{\text{appl}} \geq 12(R_0 - a) \left(\frac{L}{R_0^2} + \pi EC_m \right) \quad . \quad (C-12)$$

For the loading arrangement and specimens used in the present experiments, the machine compliance is on the order of $2-3 \times 10^{-8} \text{ m/N}$, so that the term πEC_m is much larger (1.3×10^4 to 1.9×10^4) than the term L/R_0^2 (~ 100). It follows that T_{appl} is at least on the order of 440 to 650. As before, we obtain the tearing modulus T_0 for HSSI 72W weld material at 0°C from the slope of Figure 14 at $\Delta a = 0$ together with a value of the flow stress estimate σ_{flow} of 568 MPa from Table A-1. Then

* P. C. Paris, H. Tada, A. Zahor, and H. Ernst. "The Theory of Instability of the Tearing Mode of Elastic-Plastic Crack Growth." pp. 5-36 in *Elastic-Plastic Fracture*. ASTM STP 668, J. D. Landes, J. A. Begley, and G. A. Clarke, Eds., American Society for Testing and Materials, 1979.

$$T_0 = \frac{dJ}{da} \frac{E}{\sigma_{\text{flow}}^2} \cong 462 \quad (\text{C-13})$$

Comparison of Equations (C-12) and (C-13) indicates that the initiated crack should be unstable or close to unstable in our experiments ($T_0 = 462$ $T_{\text{appl}} = 440 - 650$).

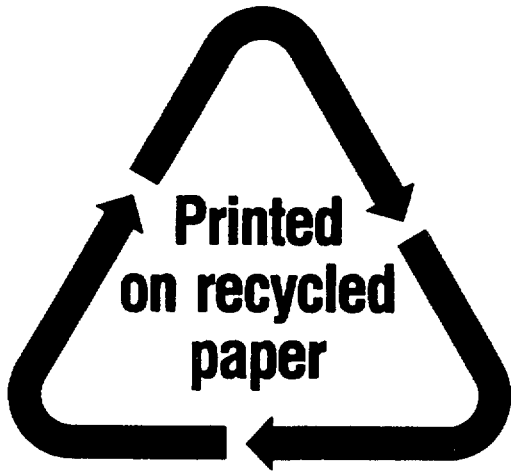
The three analyses presented in this appendix support the assumption that for the material and specimen size and geometry tested in this project, fracture initiation occurs at or very near maximum load.

CONVERSION FACTORS^a

SI unit	English unit	Factor
mm	in.	0.0393701
cm	in.	0.393701
m	ft	3.28084
m/s	ft/s	3.28084
kN	lb _f	224.809
kPa	psi	0.145038
MPa	ksi	0.145038
MPa•√m	ksi•√in.	0.910048
J	ft•lb	0.737562
K	°F or °R	1.8
kJ/m ²	in.-lb/in. ²	5.71015
W•m ⁻³ •K ⁻¹	Btu/h•ft ² •°F	1.176110
kg	lb	2.20462
kg/m ³	lb/in. ³	3.61273 × 10 ⁻⁵
mm/N	in./lb	0.175127
T(°F) = 1.8(°C) + 32		

^aMultiply SI quantity by given factor to obtain English quantity.

NRC FORM 335 (2-89) NRCM 1102, 3201, 3202	U.S. NUCLEAR REGULATORY COMMISSION	1. REPORT NUMBER (Assigned by NRC, Add Vol., Supp., Rev., and Addendum Numbers, if any.)				
BIBLIOGRAPHIC DATA SHEET <i>(See instructions on the reverse)</i>		NUREG/CR-6342 ORNL/SUB/94-DHK60				
2. TITLE AND SUBTITLE		3. DATE REPORT PUBLISHED				
Fracture Toughness Testing With Cracked Round Bars: Feasibility Study		<table border="1" style="width: 100%;"> <tr> <td style="width: 50%;">MONTH</td> <td style="width: 50%;">YEAR</td> </tr> <tr> <td style="text-align: center;">April</td> <td style="text-align: center;">2000</td> </tr> </table>	MONTH	YEAR	April	2000
MONTH	YEAR					
April	2000					
5. AUTHOR(S)		4. FIN OR GRANT NUMBER L1098				
J.H. Giovanola, J.E. Crocker		6. TYPE OF REPORT				
8. PERFORMING ORGANIZATION - NAME AND ADDRESS <i>(If NRC, provide Division, Office or Region, U.S. Nuclear Regulatory Commission, and mailing address; if contractor, provide name and mailing address.)</i>		Technical				
SRI International Poulter Laboratory 333 Ravenswood Avenue Menlo Park, CA 94025	Under Contract to: Oak Ridge National Laboratory Oak Ridge, TN 37831-6285	7. PERIOD COVERED <i>(Inclusive Dates)</i>				
9. SPONSORING ORGANIZATION - NAME AND ADDRESS <i>(If NRC, type "Same as above"; if contractor, provide NRC Division, Office or Region, U.S. Nuclear Regulatory Commission, and mailing address.)</i>						
Division of Engineering Technology Office of Nuclear Regulatory Research U. S. Nuclear Regulatory Commission Washington, DC 20555-0001						
10. SUPPLEMENTARY NOTES						
C. J. Fairbanks, NRC Project Manager						
11. ABSTRACT <i>(200 words or less)</i>						
The feasibility of measuring fracture toughness of pressure vessel steels using small-cracked round bars (CRBs) was evaluated. Data from the small CRBs were compared with similar results from 1T-compact tension specimens. Reasonably good agreement was found in the mid transition region but the CRBs produced evaluated toughness values in the low transition region.						
12. KEY WORDS/DESCRIPTORS <i>(List words or phrases that will assist researchers in locating the report.)</i>		13. AVAILABILITY STATEMENT				
fracture toughness testing precracked round bars subsized specimens pressure vessels transition temperature		unlimited				
15. NUMBER OF PAGES		14. SECURITY CLASSIFICATION <i>(This Page)</i>				
16. PRICE		unclassified				
15. NUMBER OF PAGES		<i>(This Report)</i>				
unclassified		15. NUMBER OF PAGES				



Federal Recycling Program

UNITED STATES
NUCLEAR REGULATORY COMMISSION
WASHINGTON, D.C. 20555-0001



FIRST CLASS MAIL
POSTAGE AND FEES PAID
USNRC
PERMIT NO. G-67